THE TERRESTRIAL RING CURRENT: ORIGIN, FORMATION, AND DECAY

Ioannis A. Daglis,[1] Richard M. Thorne,[2]
Wolfgang Baumjohann,[3] and Stefano Orsini[4]

Abstract. The terrestrial ring current is an electric current flowing toroidally around the Earth, centered at the equatorial plane and at altitudes of ~10,000–60,000 km. Changes in this current are responsible for global decreases in the Earth's surface magnetic field, which are known as geomagnetic storms. Intense geomagnetic storms have severe effects on technological systems, such as disturbances or even permanent damage to telecommunication and navigation satellites, telecommunication cables, and power grids. The main carriers of the storm ring current are positive ions, with energies from ~1 keV to a few hundred keV, which are trapped by the geomagnetic field and undergo an azimuthal drift. The ring current is formed by the injection of ions originating in the solar wind and the terrestrial ionosphere. The injection process involves electric fields, associated with enhanced magnetospheric convection and/or magnetospheric substorms. The quiescent ring current is carried mainly by protons of predominantly solar wind origin, while geospace activity tends to increase the abundance (both absolute and relative) of O^+ ions, which are of ionospheric origin. During intense magnetic storms, the O^+ abundance increases dramatically, resulting in a rapid intensification of the ring current and an O^+ dominance around storm maximum. This compositional change affects, among other processes, the decay of the ring current through the species- and energy-dependent charge exchange and wave-particle scattering loss. Energetic neutral atoms, products of charge exchange, enable global imaging of the ring current and are the most promising diagnostic tool of ring current evolution. This review will cover the origin of ring current particles, their transport and acceleration, the effects of compositional variations in the ring current, the effects of substorms on ring current growth, and the dynamics of ring current decay with an emphasis on the process of charge exchange and the potential for wave scattering loss.

1. INTRODUCTION

At the turn of the century, *Fitzgerald* [1892] and *Lodge* [1900] argued that a flying cloud of charged atoms emitted from sunspots caused terrestrial magnetic storms, a term coined by A. von Humboldt in 1808 [see *Tsurutani et al*., 1997]. This suggestion led *Schmidt* [1917] and *Chapman* [1919] to propose that the magnetic field depression during the main phase of magnetic storms was due to electrical currents flowing near the Earth, which were fed by charged particle streams originating at the Sun. Chapman had originally proposed a singly-charged stream, which invoked the fruitful criticism of F. Lindemann. *Lindemann* [1919] pointed out that mutual electrostatic repulsion would destroy a singly charged stream, and proposed an electrically neutral solar stream containing charged particles of both signs in equal numbers. This critically important suggestion was adopted by Chapman and led to his later work, which is the foundation of modern theories on magnetic storms.

The publications of Chapman and Ferraro in the early 1930s suggested a transient stream of outflowing solar ions and electrons responsible for terrestrial magnetic storms; once the solar stream had reached the Earth, charged particles would leak into the *magnetosphere* and drift around the Earth, creating a current whose field would oppose the main geomagnetic field [*Chapman and Ferraro*, 1930, 1931]. (Terms in italic type are defined in the glossary following the main text.) This is surprisingly close to what we believe today. The only major element of Chapman's theory that changed is the existence of a continuous (instead of transient) stream of ionized gas from the Sun. This stream was named solar wind by *Parker* [1958], and its existence was later confirmed from observations made by the Venus-heading Mariner 2 spacecraft [*Neugebauer and Snyder*, 1962; *Snyder and Neugebauer*, 1964].

Just prior to the discovery of the radiation belts by Explorer 3 [*Van Allen et al*., 1958], *Singer* [1956] proposed that particles arriving from the Sun could, by

[1]Institute of Ionospheric and Space Research, National Observatory of Athens, Penteli, Greece.
[2]Department of Atmospheric Sciences, University of California, Los Angeles.
[3]Max-Planck-Institut für Extraterrestrische Physik, Garching, Germany.
[4]Istituto di Fisica dello Spazio Interplanetario, Consiglio Nazionale delle Ricerche, Rome.

Reviews of Geophysics, 37, 4 / *November 1999*
pages 407–438
8755-1209/99/1999RG900009*$15.00*
Paper number 1999RG900009

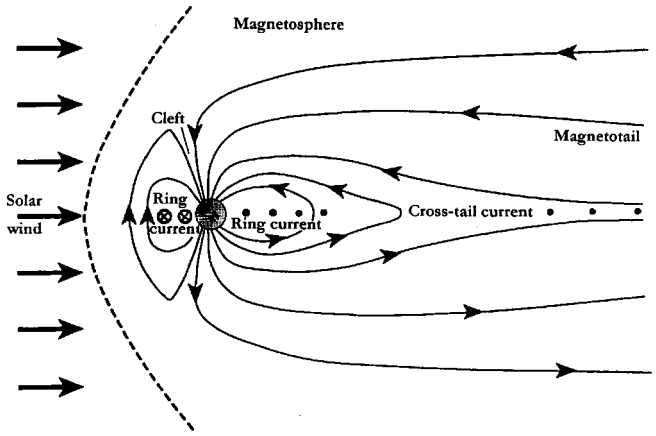

Figure 1. Schematic outline of the terrestrial magnetosphere.

collective motion, perturb the dipolar magnetic field of the Earth sufficiently to allow entry of the particles into the trapping regions identified by *Størmer* [1955]. A more detailed theory followed [*Singer*, 1957], suggesting that the gradient drift of the energetic particles trapped in the geomagnetic field carries a westward electric current, which effectively decreases the horizontal component of the magnetic field in the vicinity of the Earth. Thus the existence of a ring current was inferred before the dawn of the spaceflight era.

The ring current is the key element of magnetic storms in the near-Earth space (see the schematic of the terrestrial magnetosphere in Figure 1). In recent years there has been a wider interest in magnetic storms owing to the severe effects they have on technological systems. Relevant reports refer to disturbances or even permanent damage of telecommunication and navigation satellites, telecommunication cables, and power grids [e.g., *Lanzerotti*, 1994; *Kappenman et al*., 1997]. Moreover, the case of magnetic storm effects on terrestrial climate [*Baker et al*., 1993; *Burns et al*., 1995; *Tinsley*, 1996] and on human physiology has been addressed recently [*Breus et al*., 1995; *Roederer*, 1995].

2. GENERAL STRUCTURE OF THE RING CURRENT

The ring current can be envisioned as a toroidal-shaped electric current that flows westward around the Earth, with variable density at geocentric distances between $\sim 2\ R_E$ and $\sim 9\ R_E$.

Geomagnetically trapped charged particles, which gyrate around the ambient field as a result of the Lorentz force, are also subject to drift motions owing to the gradient and curvature of the magnetic field [*Baumjohann and Treumann*, 1996]. The total effect is a collective azimuthal drift, which is oppositely directed for ions and electrons: electrons move eastward and most ions (with energies above a relatively low threshold [see *De Michelis et al*., 1997]) move westward. This drift constitutes a net charge transport; the current associated with the charge transport is the ring current.

The basic motions of charged particles in the presence of a magnetic field are the gradient drift motion, the curvature drift motion and the gyration (see Figure 2 and *Baumjohann et al*. [1996]). The elementary currents $\mathbf{j}_\nabla$, $\mathbf{j}_C$, and $\mathbf{j}_G$ resulting from these motions can be expressed in terms of particle pressure perpendicular ($P_\perp$) and parallel ($P_\parallel$) to the magnetic field, as first established by *Parker* [1957]. The current due to particle drift driven by the magnetic field gradient is

$$\mathbf{j}_\nabla = P_\perp \frac{\mathbf{B} \times \nabla B}{B^3} \tag{1}$$

The current due to particle drift driven by the magnetic field curvature is expressed as

$$\mathbf{j}_C = \frac{P_\parallel}{B^4} \mathbf{B} \times (\mathbf{B} \cdot \nabla)\mathbf{B} \tag{2}$$

while the current due to *gyration* effects within the particle distribution is

$$\mathbf{j}_G = \frac{\mathbf{B}}{B^2} \times \left(\nabla P_\perp - \frac{P_\perp}{B} \nabla B - \frac{P_\perp}{B^2} (\mathbf{B} \cdot \nabla)\mathbf{B} \right) \tag{3}$$

The three terms on the right side of (3) represent currents due to the particle pressure gradient, the magnetic field gradient, and the magnetic field line curvature, respectively. Since the drift and gyration terms driven by the magnetic field gradient are equal and opposite (equations (1) and (3)), the total current does not depend on gradients of the magnetic field:

$$\mathbf{j} = \mathbf{j}_\nabla + \mathbf{j}_C + \mathbf{j}_G = \frac{\mathbf{B}}{B^2} \times \left(\nabla P_\perp + \frac{P_\parallel - P_\perp}{B^2} (\mathbf{B} \cdot \nabla)\mathbf{B} \right) \tag{4}$$

In the case of an isotropic ($P_\parallel = P_\perp$) distribution, or a straight magnetic field line geometry, the magnetic field configuration plays no role in the current buildup. The current system is then established only by particle pressure gradients.

The quiet time ring current population is distributed

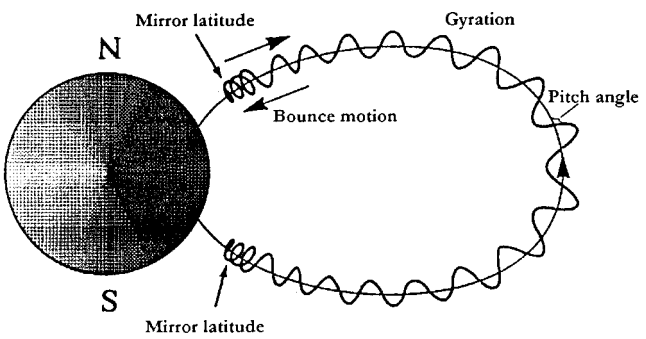

Figure 2. Cyclotron motion (gyration) and bounce motion of a charged particle along a geomagnetic field line.

over the *L parameter* range ~2–9, with average current density values of ~1–4 nA m^{-2} [e.g., *Lui et al*., 1992; *De Michelis et al*., 1997]. The storm time ring current density increases over its whole radial extent, and may exceed current density values of ~7 nA m^{-2} [e.g., *Lui et al*., 1987].

Dessler and Parker [1959] and *Sckopke* [1966] showed theoretically that the disturbance ΔB of the equatorial surface geomagnetic field during magnetic storms is proportional to the energy of the ring current particles:

$$\frac{\Delta B}{B_0} = \frac{2E}{3E_m} \tag{5}$$

where B_0 is the average surface geomagnetic field intensity at the magnetic equator (~0.3 G), E is the total energy of the ring current particles and $E_m = B_0^2 R_E^3/3 \simeq 10^{18}$ J, is the energy of the Earth's dipole field above the Earth's surface [*Carovillano and Siscoe*, 1973].

The generalized Dessler-Parker-Sckopke relation includes terms from internal and boundary sources:

$$\frac{B_D}{B_0} = \frac{2E + M - \oint \mathbf{R} \cdot \mathbf{n}\, d\sigma}{3E_m} \tag{6}$$

where B_D is the field decrease due to the combined magnetic field from all sources (the ring current, the magnetopause current and the magnetotail current); M is the total magnetic energy inside the magnetosphere, that is the volume integral of $B_D^2/2\mu_0$. The unit vector $\mathbf{n}$ is the outward pointing normal, and $\mathbf{R}$ is

$$\mathbf{R} = \left(p + \frac{B^2}{2\mu_0}\right)\mathbf{r} + \rho(\mathbf{V} \cdot \mathbf{r})\mathbf{V} - \frac{(\mathbf{B} \cdot \mathbf{r})\mathbf{B}}{\mu_0} \tag{7}$$

In (7), p is the thermal pressure, $\mathbf{r}$ is the radius vector from the center of the Earth, ρ is the mass density of the *solar wind* in the plasma mantle, $\mathbf{V}$ is the flow velocity of the mantle plasma, and $\mathbf{B}$ is the total magnetic field vector (dipole field plus magnetospheric field). The pressure is assumed to be isotropic.

Theoretical and observational work established the general location and the driving forces of this current system. Spacecraft measurements that confirmed the existence of the ring current also showed that it is a permanent feature. *Frank* [1967] showed that the ring current is dominated by ions (presumably protons) with energies of ~50 *keV*. The development of mass-resolving space instrumentation in the 1970s made it possible to distinguish between ionic species in space [*Shelley et al*., 1972]. However, the detailed composition and energy of the ring current were not clarified until the Active Magnetospheric Particle Tracer Explorer (AMPTE) mission of the late 1980s (section 3.1).

3. SOURCES OF RING CURRENT PARTICLES

Although all trapped particles in the inner magnetosphere contribute to the ring current, only ions in the medium-energy range of ~10 keV to a few hundreds of keV contribute substantially to the total current density [*Williams*, 1987]. Electrons contribute little to the ring current on account of their negligible energy density [*Baumjohann*, 1993]. The immediate particle sources of the ring current are the magnetospheric *plasma sheet* and the terrestrial *ionosphere*. The plasma sheet population is supplied by the ionosphere and the solar wind. Hence the ultimate main sources of ring current particles are the solar wind and the terrestrial ionosphere.

Magnetospheric H^+ ions originate both in the ionosphere and in the solar wind; this complicates the identification of the dominant source. In contrast, the vast majority of magnetospheric O^+ originates in the ionosphere. *Charge exchange* processes (section 5) in the inner magnetosphere further complicate matters because they transform higher charge state oxygen ions (of solar wind origin) to ionosphere-like lower charge state oxygen, and solar wind He^{++} into He^+ (which is provided also by the ionosphere). However, only a negligible percentage of magnetospheric O^+ ions originates through charge exchange from solar wind oxygen ions with high charge states (O^{6+}). Therefore O^+ ions are considered tracer ions of ionospheric outflow associated with magnetosphere-ionosphere coupling.

On the basis of high O^{++}/O^+ and/or high He^+/He^{++} ratios, which are not observed in either the solar wind or the ionosphere in the range of a few keV, it has been argued that the *plasmasphere* is also a direct source of ring current ions [*Balsiger et al*., 1980]. However, it is a minor source, since O^{++} and He^+ are found only in small numbers in the ring current.

Until the end of the 1980s there was considerable uncertainty regarding the sources of ring current ions. In the early years of space exploration it was generally assumed that solar wind protons penetrate and dominate the magnetosphere. Accordingly, the ring current was considered a solar-origin proton current. The contribution of the terrestrial ionosphere was regarded as negligible. This assumption was due mainly to the low initial energy of ionospheric ions, which is of the order of several eV to several tens of eV, compared with the higher initial energy of solar wind ions, which is of the order of several keV. It was also due to the inability of the first generation of space-based measuring devices to provide full identification (mass and charge state) of the detected ions. The lack of compositional information led to the erroneous conclusion that essentially all ions in geospace are protons of solar wind origin. Opposing theories [*Dessler and Hanson*, 1961; *Axford*, 1970] were discarded for lack of supporting observations.

In the early 1970s the solar origin theory was challenged by the discovery of energetic heavy ions (M/q = 16) at energies up to 17 keV [*Shelley et al*., 1972] by the

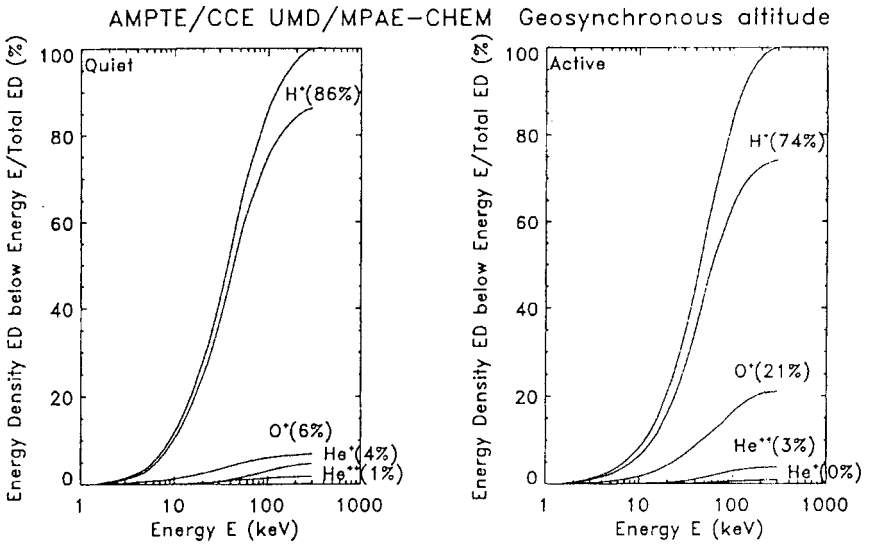

Figure 3. Accumulated percentage of the ion energy density at geosynchronous altitude (i.e., outer ring current) as a function of energy, (left) at geomagnetically quiet times and (right) at active times [*Daglis et al*., 1993]. Plotted are curves for the total energy density as well as for the energy density of the four main ion species (H^+, O^+, He^{++}, and He^+). Details are given in the text. Reprinted with permission from Springer-Verlag Inc.

first mass spectrometer in space, on board the polar-orbiting satellite 1971-089A. These ions were presumably O^+ ions originating in the terrestrial ionosphere. In the following years, a new type of ion composition instrumentation made it possible to obtain charge state information in addition to M/q analysis of energetic ions [*Gloeckler and Hsieh*, 1979]. Observations by the missions GEOS 1 and 2, Prognoz 7, and SCATHA confirmed the existence of O^+ in the magnetosphere, and the significant contribution of the ionospheric source during magnetic storms [*Balsiger et al*., 1980; *Lundin et al*., 1980; *Kaye et al*., 1981]. Because O^+ ions are not found in the solar wind and are abundant in the ionosphere, they have since been used as evidence and as a measure of ionospheric contribution to any magnetospheric population.

However, early composition observations existed only in the low (≤15 keV) and high (≥600 keV) energy portion of the ring current energy density distribution [*Williams*, 1980, 1981]. The lack of composition information at intermediate energies was critical, since the ring current energy distribution has its maximum value within this energy range [*Smith and Hoffman*, 1973; *Williams*, 1983]. In particular, *Williams* [1980] estimated that the bulk (~90%) of the ring current is contained in the 15- to 250-keV energy range [see *Williams*, 1983, Figure 5] and that the mean energy of the ring current is several tens of keV. Moreover, *Williams* [1980] noted that no information at all (either direct measurements or inferences) existed concerning the peak (50–100 keV) of the ring current energy density distribution. The estimates of *Williams* [1980] were confirmed by the AMPTE mission [*Williams*, 1987]. AMPTE was the first mission to adequately measure the composition of the main part of the ring current.

3.1. Conclusive Ring Current Measurements

Launched on board the Charge Composition Explorer (CCE), one of the three AMPTE spacecraft [*Krimigis et al*., 1982], the charge-energy-mass (CHEM) spectrometer was used to identify missing elemental and charge composition over the range of a few keV to a few hundred keV. CHEM was an advanced composition spectrometer that used a combination of measurement techniques [*Gloeckler et al*., 1985b]. Case studies [*Gloeckler et al*., 1985a; *Krimigis et al*., 1985; *Hamilton et al*., 1988], and statistical studies of the ion population in the inner magnetosphere [*Daglis et al*., 1993] clarified the relative contribution of the various ion species to the quiet time and storm time ring current. Figure 3 is adopted from *Daglis et al*. [1993] and shows both the contribution of the different ion species to the total energy density and the energy distribution of the ion energy density. The curves represent averages over 2.5 years of measurements by the CHEM instrument onboard AMPTE/CCE. They show the accumulated percentage of the ion energy density at geosynchronous altitude (i.e., outer ring current) as a function of energy. Plotted are curves for the total energy density as well as the energy density of the four main ion species (H^+, O^+, He^{++}, He^+). The left panel shows the average energy density distribution in the outer ring current at geomagnetically quiet times, while the right panel shows the average distribution for active times. There are two outstanding features: First, the bulk of the total measured ion energy density is contained in the energy range ~10–100 keV; second, H^+ is the dominant ion species, with the O^+ contribution increasing drastically (from 6% to 21%) during active times. It should be stressed that these numbers are averages over all local times and over all kinds of events (storms/*substorms*) with *auroral electrojet* (*AE*) *indices* $AE < 30$ nT (quiet times) and $AE > 700$ nT (active times). This means that the characteristics of intense events (for example, the February 1986 storm, which is mentioned in the next paragraph) are smoothed out. We should also note that according to previous ring current measurements covering energies above 300 keV, a nonnegligible percentage (~5%) of

the energy density resides at energies >300 keV [*Williams*, 1987, Figure 1].

In summary, the AMPTE mission showed that protons are the dominant ion species in the quiet time ring current, with the contribution of ions heavier than protons being essentially negligible. Because AMPTE operated during solar minimum, there was only one intense magnetic storm to be observed. This storm occurred in February 1986 and was studied in detail by *Hamilton et al*. [1988]. It was shown that the abundance of O^+ not only rose continuously during the storm, but eventually became the dominant ion species near the storm's maximum phase, contributing 47% of the total energy density in the inner ring current (L = 3–5), compared with 36% in H^+. The situation in the outer ring current (L = 5–7) was less dramatic: the maximum O^+ contribution there was 31%, with H^+ contributing 51% at that time [see *Hamilton et al*., 1988, Figure 4].

The second highly favorable mission for conducting ring current investigations was the Combined Release and Radiation Effects Satellite (CRRES), which operated during 1990–1991, i.e., around solar maximum. The Magnetospheric Ion Composition Spectrometer (MICS; see *Wilken et al*. [1992] for details) on board CRRES had the capability, like CHEM on board AMPTE/CCE, to obtain compositional information for the bulk of the ring current ions, that is, for the energy range between a few tens of keV to a few hundred keV. CRRES/MICS observations of several moderate and large magnetic storms showed that the ring current characteristics observed by CCE/CHEM in the February 1986 storm [*Hamilton et al*., 1988] are common. *Daglis* [1997a] showed that the larger the storm is (as quantified by the *Dst index*), the larger the O^+ contribution to the ring current. Moreover, *Daglis* [1997a] showed that the *Dst* magnitude and the O^+ contribution to the ring current increase concurrently. This feature was present in all moderate to large storms during 1991, and it was also noticed in the February 1986 storm by *Hamilton et al*. [1988].

Figure 4 shows the time profiles of compositional changes and of the *Dst* index during the June 4–5, 1991, storm. We use a special high-resolution (5 min) *Dst* index here, which was produced by the Solar-Terrestrial Environment Laboratory, Nagoya University (courtesy Y. Kamide). The top two panels show the contribution of the two main ion species H^+ and O^+ to the total energy density of the outer ring current population (L range of 5–6). The actual contribution of the main ion species cannot be calculated from the MICS count rates below $L \approx 5$ owing to the operation of the particle identifier (PID) at lower altitudes. PID is a fast analog processor evaluating the sensor information, with the purpose of preventing high H^+ fluxes from overloading the relatively slow analog-to-digital conversion of the sensor signals [*Wilken et al*., 1992]. As a result, the mass/mass-per-charge matrix count rates are affected by the PID, in the sense that the H^+ rates are close to zero.

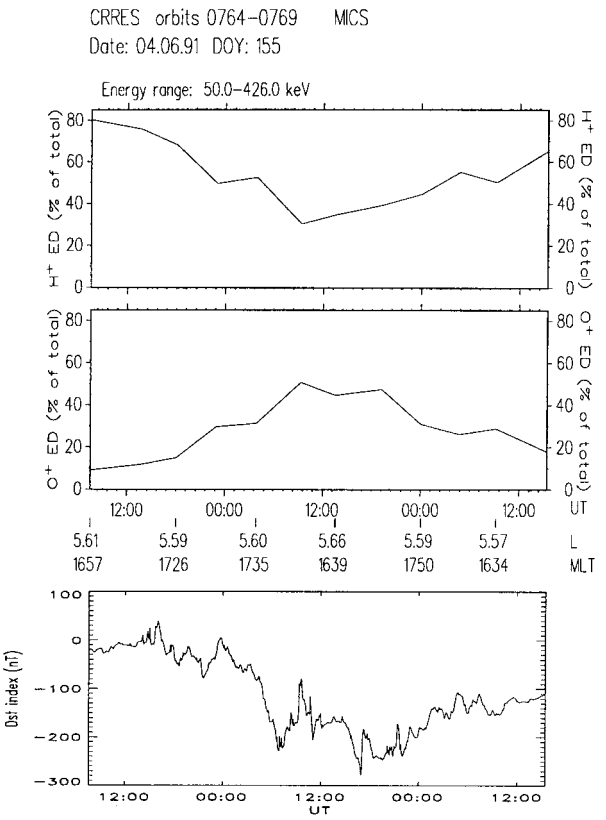

Figure 4. Time profiles of (top) the H^+ and O^+ contributions to the total ion energy density in the ring current at L = 5–6, and (bottom) the 5-min *Dst* index during the intense storm of June 5, 1991.

In Figure 4 we can see that the prestorm passes of CRRES through the outer ring current region recorded a "normal" relation of H^+ and O^+: H^+, being the dominant ion species contributed ~80%, and O^+ contributed only ~10% of the measured ion energy density. After the start of the storm, the O^+ contribution rose steadily and remained above 30%, an exceptionally high level [*Daglis et al*., 1993], for more than 24 hours. Energetic O^+ enhancements are usually short-lived [*Daglis et al*., 1996], presumably because of the localized and sporadic character of ionospheric outflow [e.g., *Kaye et al*., 1981; *Strangeway and Johnson*, 1983]. Moreover, the charge exchange lifetime of energetic O^+ is relatively short: 100-keV O^+ ions have a lifetime of ~33, 22, and 11 hours at L = 5.0, 4.25, and 3.5 respectively [*Smith and Bewtra*, 1978; *Smith et al*., 1981]. Therefore the long-lived enhanced level of O^+ abundance indicates a continuous ionospheric feeding of the inner plasma sheet during the storm main phase.

During the great storm in March 1991, the increase of the O^+ abundance was overwhelming (Figure 5). O^+ clearly dominated around the maximum of the main phase. Its contribution was more than 65% of the total energy density in the L range 5–7, while it exceeded 80% in the L range 5–6 [*Daglis et al*., 1999a]. *Daglis* [1997a] commented on the especially interesting concurrent in-

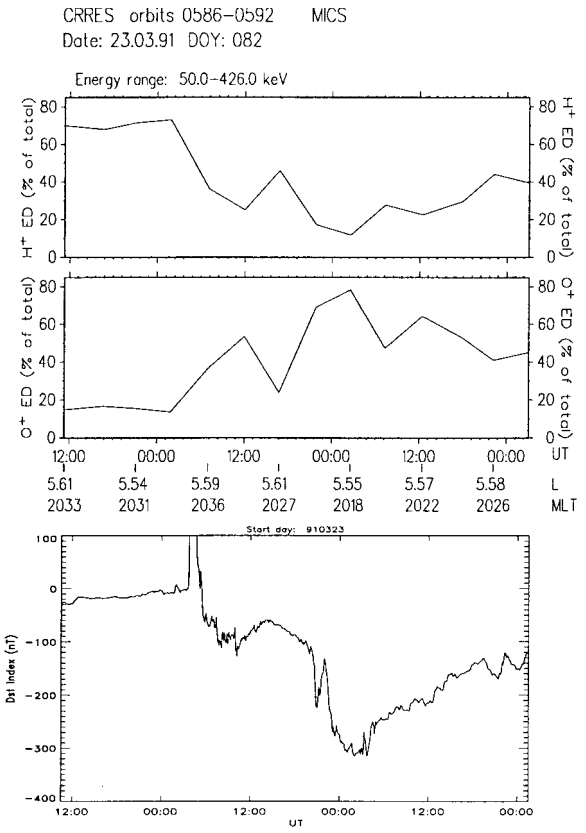

Figure 5. The great magnetic storm of March 24, 1991: time profiles of (top) the H^+ and O^+ contributions to the total ion energy density in the ring current region at L = 5–6 (as measured by CRRES-MICS, and (bottom) the 5-min *Dst* index. The main features to be observed are the dominance of O^+ during storm maximum and the concurrent increase of the $|Dst|$ level and of the O^+ contribution to the total ion energy density. Reprinted from *Daglis et al.* [1999a] with permission from Elsevier Science.

crease of the O^+ contribution and the *Dst* magnitude. After the storm sudden commencement at 0341 UT on March 24, the O^+ contribution rose from the ~10% level to the ~40% level, while at the same time *Dst* dropped to about −100 nT. A period of transient *Dst* recovery and O^+ decrease followed. During the main phase of the storm, both *Dst* and O^+ reached their peaks. A similar pattern was observed in the great storm of February 1986 [*Hamilton et al.*, 1988]. Figure 5 shows that the O^+ contribution remains at an extraordinary high level (>40%) for a very extended time period (>30 hours).

In 1991, CRRES observed five medium to intense storms. During all of them the purely ionospheric part of the ring current, as represented by energetic O^+ ions, was 20–65% (in terms of energy density). Taking into account that ~30% of H^+ in the storm time outer ring is also of ionospheric origin [*Gloeckler and Hamilton*, 1987], it is clear that, although the energy source of storms is unambiguously of solar origin, the majority of the storm time ring current particles are of terrestrial origin. Hence one can conclude that the major source of the quiet time ring current is the solar wind (via the storage region of the plasma sheet), while the storm time ring current is increasingly terrestrial in origin. *Daglis* [1997b] suggested that the role of O^+, the major outflowing ionospheric ion, in the evolution of intense storms is twofold (Figure 6):

1. It causes the rapid final enhancement of the ring current at storm maximum. This could be the cause of the second storm maximum during intense storms with a two-step development [*Kamide et al.*, 1998a].
2. It induces an equally rapid initial decay of the ring current [e.g., *Noël*, 1997a, b]. This is presumably the cause of the two-step recovery of intense storms. Both points are further discussed in section 3.2.3.

In summary, the main sources of ring current particles are the solar wind and the terrestrial ionosphere. The quiet time ring current is dominated by protons (see Table 1). The only other ion species that contributes substantially to the ring current is O^+, which becomes increasingly important with geomagnetic activity, and eventually dominates the ring current during great storms [*Daglis*, 1997a, b]. Typical values of O^+ contribution to the ring current energy density are ~6% during quiet time and more than 50% during great storms. Essentially all of the ring current O^+ ions originate in the high-latitude ionosphere of the Earth. The origin of the ring current protons is less clear. For the quiet time ring current, *Gloeckler and Hamilton* [1987] estimated that ~35% of protons in the outer ring current (L =

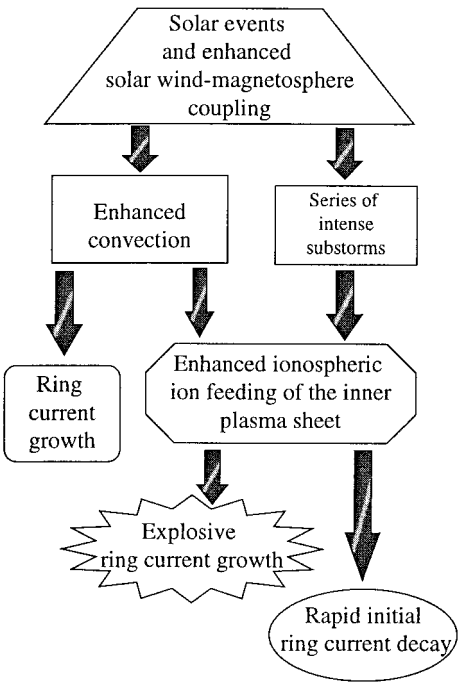

Figure 6. Twofold role of O^+, the major outflowing ionospheric ion, in the evolution of intense storms. It both (1) causes the rapid final enhancement of the ring current at storm maximum and (2) induces an equally rapid initial ring current decay [*Daglis*, 1997b, Figure 3].

5–7) and ~75% of protons in the inner ring current (L = 3–5) are of ionospheric origin. For the storm time ring current, *Gloeckler and Hamilton* [1987] estimated that ~30% of protons in the outer ring current and ~65% of protons in the inner ring current are of ionospheric origin. Solar wind He^{++} ions usually contribute less than 4% of the ring current, except in the case of great storms (see Table 1).

3.2. The Sources: Geometry, Transport and Acceleration

The solar wind and the terrestrial ionosphere are the two substantial sources of ring current ions. Their relative strength for three different conditions are summarized in Table 1. Table 1 is a compilation based on composition measurements by the AMPTE/CCE and the CRRES missions [*Gloeckler et al*., 1985a; *Gloeckler and Hamilton*, 1987; *Hamilton et al*., 1988; *Daglis et al*., 1993; *Daglis*, 1997a] during quiet times, small–medium storms, and intense storms. The values are calculated using observations at $L \approx 5$, which is near the maximum of the current density of the ring current [*Lui et al*., 1987; *De Michelis et al*., 1997].

3.2.1. Solar wind. With an impressive source strength of several 10^{29} ions s^{-1} incident on the magnetosphere, the solar wind had been the indisputable candidate of magnetospheric plasma supply for many years. The entry of 0.1–1.0% of the incident particles into the magnetosphere results in an effective solar wind source strength of 10^{26}–10^{27} ions s^{-1}. Not until the late 1980s was the prominent position of the solar wind threatened by the terrestrial ionosphere. Then *Chappell et al*. [1987] summarized ionospheric outflow observations and suggested that the ionosphere is able to supply essentially all magnetospheric plasma under any geomagnetic condition.

Recently, however, measurements from the Geotail mission [*Nishida*, 1994] confirmed the importance of the solar wind source for energetic ions in the magnetotail, especially for distances greater than ~30 R_E [*Christon et al*., 1996]. Investigation of combined measurements from the Wind and Geotail spacecraft [*Terasawa et al*., 1997] showed that for extended periods of northward *interplanetary magnetic field* (*IMF*), that is, during geomagnetically quiet times, the magnetotail at distances beyond 15 R_E is dominated by solar wind particles entering through the flank regions. This reinforces the conclusions of *Lennartsson and Shelley* [1986] and *Gloeckler et al*. [1984] on the dominant role of the solar wind source in the magnetotail. Radial profiles of ion charge states in the near-Earth plasma sheet also confirm the increasing solar wind source strength toward higher altitudes [*Christon et al*., 1994].

However, despite our general knowledge about the relative strength of the solar wind source with respect to altitude, and despite the existence of some successful relevant models [e.g., *Pilipp and Morfill*, 1978], the effective source geometry of the solar wind, that is, where and how solar wind particles enter the magnetosphere, remains an open question. Also largely unknown are the transport and acceleration processes acting on these particles, before they reach the inner magnetosphere to contribute to the ring current. The complexity of the transport is illustrated by the fact that mixing of the ionospheric and the solar wind source has been observed to distances of ~210 R_E down the magnetotail [*Hirahara et al*., 1996; *Seki et al*., 1996].

TABLE 1. Sources of Ring Current Ions, According to Composition Measurements by the AMPTE and CRRES Missions: Contribution of Main Ion Species to Total Ion Energy Density at $L \approx 5$

Ion Source and Species	*Quiet Time*	*Small–Medium Storms*	*Intense Storms*
Total energy density, keV cm^{-3}	~10	≥50	≥100
Solar wind H^+, %	≥60	~50	≤20
Ionospheric H^+, %	≥30	~20	≤10
Ionospheric O^+, %	≤5	~30	≥60
Solar wind He^{++}, %	~2	≤5	≥10
Solar wind He^+, %	<1	<1	<1
Ionospheric He^+, %	<1	<1	<1
Solar wind, total, %	~65	~50	~30
Ionosphere, total, %	~35	~50	~70

The acceleration of particles from the magnetotail toward the inner magnetosphere was first addressed by *Speiser* [1965a, b]. He demonstrated the effects of the $E \times B$ drift of the particles through the magnetotail, when encountering a realistic model neutral sheet, that is, a region with a small, finite, normal magnetic field B_n. Speiser showed that particles are efficiently accelerated and that some of them are ejected from the neutral sheet along the ambient magnetic field lines. Later work on his ideas yielded details on the complexity of particle acceleration in the magnetotail [e.g., *Lyons and Speiser*, 1982; *Speiser and Lyons*, 1984; *Chen and Palmadesso*, 1986; *Büchner and Zelenyi*, 1989]. In recent years, comprehensive modeling work has addressed the particle source issue by incorporating the nonlinear aspects of particle trajectories in the magnetotail [e.g., *Ashour-Abdalla et al*., 1993]. These modeling efforts are crucial for clarifying the acceleration and transport of (mainly solar wind origin) ions from the magnetotail to the inner magnetosphere.

3.2.2. Ionosphere. The ionosphere is a variable source of ions [*Horwitz*, 1982; *Moore*, 1984; *Hultqvist*, 1991; *Horwitz*, 1995], with a source strength of the same order as the solar wind [*Chappell et al*., 1987; *Moore and Delcourt*, 1995]. Revised estimates of ionospheric outflow prompted *Chappell et al*. [1987] to question the conclusions of *Hill* [1974] and to argue that the ionosphere alone is able to supply essentially all magnetospheric plasma. Knowledge of the source strengths alone, however, cannot provide conclusive information on the final mixture of species and on their relative

importance for the dynamic processes in the magnetosphere. Transport and acceleration processes modify these numbers. The suggestion of *Chappell et al*. [1987] was certainly important in light of the fact that the ionosphere had for a long time been underestimated, like some kind of geospace Cinderella, and it had become necessary to highlight its importance. However, the potential of the ionosphere to act as a source of magnetospheric plasma is, exactly as the potential of its rival the solar wind, limited by the transport paths and acceleration mechanisms, as observations clearly show.

The two most important ionospheric outflow regions are the dayside *cleft* and the auroral region. Recently, the high-altitude polar wind also proved to be a significant O^+ source [*Chandler et al*., 1991; *Horwitz et al*., 1992; *Abe et al*., 1993; *Ho et al*., 1994], contrary to the classic polar wind theory and older satellite observations [*Banks and Holzer*, 1969; *Hoffman and Dodson*, 1980]. The midlatitude ionosphere can also be a significant source of outflowing thermal O^+ during magnetic storms [*Yeh and Foster*, 1990].

There is a controversy on the primary region of ionospheric ion outflow. The relative importance of the auroral acceleration region and cleft ion fountain as magnetospheric ion sources remains unresolved. Observational studies have indicated the importance of both regions [*Shelley*, 1986; *Lockwood et al*., 1985; *Hultqvist et al*., 1988; *Lu et al*., 1992], and modeling studies have assessed the transport and energization of ionospheric ions, from the cleft region [*Horwitz and Lockwood*, 1985; *Delcourt et al*., 1990a; *Cladis and Francis*, 1992] as well as from the auroral region [*Shapiro et al*., 1995; *Wodnicka and Banaszkiewicz*, 1996, 1997]. Comprehensive statistical studies have established the extent of ion outflow from each region [*Yau et al*., 1984, 1985, 1986]. However, it is expected that different ionospheric regions are dominant ion outflow regions for different magnetospheric conditions and/or different levels of the solar wind–magnetosphere dynamo activity [*Daglis and Axford*, 1996]. The issue can be solved through global neutral atom imaging of the high-latitude ion outflow regions [*Hesse et al*., 1993a; *Daglis and Livi*, 1995]. Since both major ionospheric ion species O^+ and H^+ charge exchange with the exospheric neutral H [e.g., *Orsini et al*., 1994], there is an intense flux of neutral O and H in the high-latitude magnetosphere, the predominant region of ionospheric outflow to the magnetosphere [*Moore*, 1984]. *Hesse et al*. [1993b] demonstrated that neutral atom imaging of the cleft ion fountain is feasible and would lead to images of both the spatial and temporal evolution.

Since the ionospheric ions are rather cold, the question of efficient acceleration of the ionospheric ions and associated extraction into the magnetosphere is of central interest. Presumably, a variety of successive acceleration mechanisms act on the ionospheric ions to raise the particle energy from ~1 eV to tens of keV. Several satellite observations have indicated upward acceleration of ionospheric ions in auroral regions, in the form of ion beams and *ion conics* with energies of 0.1–10 keV [e.g., *Mizera and Fennell*, 1977; *Ghielmetti et al*., 1978; *Gorney et al*., 1981; *Peterson et al*., 1988]. Observations of the Swedish satellite Viking provided information on transverse and parallel ion acceleration at the topside ionosphere, both in auroral regions and in the cleft region [*Lundin et al*., 1987; *Thelin et al*., 1990]. There are several examples from the Viking data of elevated ion conics with accelerations up to the 40-keV upper limit of the ion spectrometer [*Lundin and Eliasson*, 1991]. Rocket experiments [*Kintner et al*., 1992] indicated the existence of very localized regions of intense (peak-to-peak amplitudes of 100–300 mV m^{-1}) lower hybrid waves and transversely accelerated ions with energies (10–100 eV) sufficient to eject them into the magnetosphere. Recent observations by the Swedish-German Freja satellite at low altitudes confirmed the association of the transverse energization of ionospheric ions with large depletion holes in the ionosphere [*Lundin et al*., 1994].

3.2.3. Implications of compositional changes. The fact that the various ionospheric sources remain active for several hours during storms, results in accumulation of O^+ ions, which otherwise would be impossible because O^+ ions are removed rather quickly [*Daglis and Axford*, 1996]. The compositional changes in favor of O^+ are substantial during all storms and become most prominent during intense storms [*Daglis*, 1997a]. The explosive ionospheric feeding of the magnetosphere may be the cause of the rapid second enhancement of the ring current and *Dst* depression, observed during the main phase of intense storms with a two-step development [*Kamide et al*., 1998a]. Furthermore, an O^+-loaded ring current has important differences from a proton ring current regarding wave-particle interactions and charge exchange decay.

As is discussed in more detail in section 6, the loss of ring current ions can also be influenced by wave-particle interactions. *Electromagnetic ion cyclotron* (*EMIC*) *waves*, which can be excited during storms, can cause rapid scattering loss into the atmosphere [e.g., *Cornwall et al*., 1970]. The propagation characteristics of EMIC waves and the resulting growth rates are strongly dependent on the relative ion abundance [e.g., *Kozyra et al*., 1984] at different phases of a storm. During great magnetic storms, when the injected O^+ concentration in the ring current may exceed that of H^+, the growth of EMIC waves is likely to be suppressed or confined to frequencies below the O^+ gyrofrequency [*Thorne and Horne*, 1997]. The modulation of EMIC instability by O^+ injection should therefore also change the ability of waves to provide a rapid loss process for ring current H^+ during the main phase of a storm.

Increased O^+ abundance will also influence the long-term decay rate of the ring current, since the charge exchange lifetime of O^+ is considerably shorter than the H^+ lifetime for ring current energies ≥40 keV [*Smith et*

al., 1981]. This implies that an O^+-dominated ring current will initially decay faster (Figure 6). Such a fast initial ring current decay, associated with a large O^+ component during the storm main phase, has indeed been observed in the February 1986 storm [*Hamilton et al*., 1988] and in the four intense storms observed by CRRES in 1991 [*Daglis*, 1997a]. [*Akasofu et al*., 1963] reported a two-stage recovery of intense storms as early as 1963; they suggested the existence of two ring currents around the Earth, with the one located closer to the Earth decaying faster. This could account for the different recovery profile of intense storms: a more rapid initial decay of the ring current and a decrease of the decay rate with time. However, the observations reported by *Hamilton et al*. [1988] and *Daglis* [1997a] strongly imply that the two-phase recovery of intense magnetic storms may be related to the presence of two ion components with distinctly different charge exchange lifetimes rather than to the existence of multiple, spatially separated ring currents.

Figure 7 illustrates the implications of composition- and energy-dependent charge exchange losses. The charge exchange lifetimes of the main ring current ion species, namely, H^+ and O^+, are radically different. In the energy range of several tens of keV (50–100 keV), where the bulk of the storm time ring current energy is contained, the O^+ lifetime can be 10 times shorter than that of H^+. This difference increases for higher energies. For example, at $L = 5$ and a *mirror latitude* of 14°, the charge exchange lifetime of a 100 keV O^+ ion is ~46 hours; for the same energy the lifetime of H^+ ions is ~470 hours. These timescales become considerably shorter in the inner ring current because the *geocorona* density increases. At $L = 3.5$ the respective 100 keV O^+ and H^+ lifetimes are 11 and 110 hours. In contrast, in the lower energy range, O^+ has a much longer lifetime than H^+: at $L = 5$ the 10 keV O^+ and H^+ lifetimes are ~56 hours and ~17 hours respectively, and at $L = 3.5$ the lifetimes become 28 and 5.5 hours, respectively. The implications of these differences are very important. A large (not to mention a dominant) O^+ component will induce (1) a rapid initial decay, just after the storm maximum, due to the rapid loss of high-energy O^+, and (2) a decrease of the decay rate during the recovery phase, due to the relatively long lifetimes of low-energy O^+.

It is obvious that ion composition is crucial in the dynamic evolution of the ring current. Variations in the relative abundance of the two main ion species H^+ and O^+ may regulate the decay rate of the storm time ring current [*Tinsley and Akasofu*, 1982] and should be taken into account in any comprehensive modeling study.

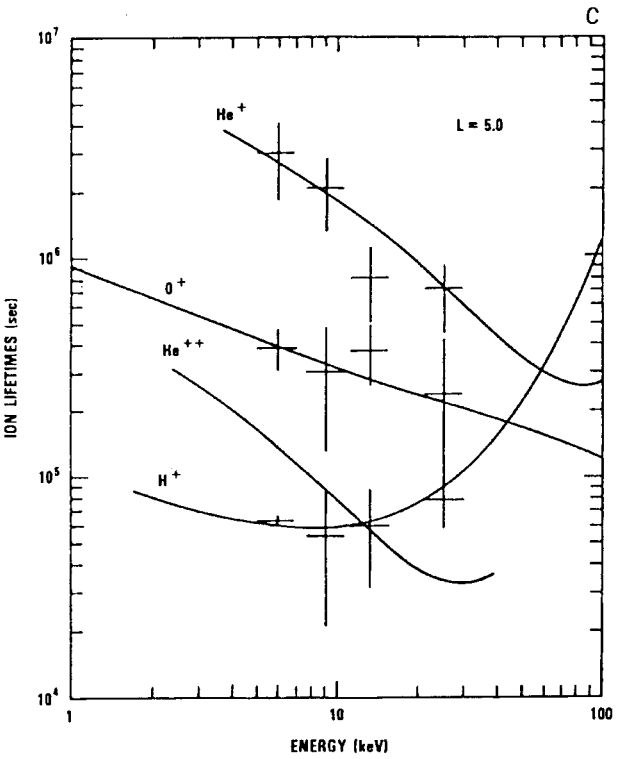

Figure 7. Measured (crosses) and predicted (curves) charge exchange lifetimes in seconds for H^+, O^+, He^{++}, and He^+ in the energy range of 1–100 keV, at $L = 5$ [*Smith et al*., 1981].

4. THE ROLE OF SUBSTORMS IN THE FORMATION OF THE RING CURRENT

The ring current is formed primarily through injection and subsequent trapping of particles from the plasma sheet into the inner magnetosphere. Injection of the particles is driven by strong duskward electric fields. A controversy still exists regarding the formation process of the storm time ring current: it is the question of whether the injection of particles results mainly from potential electric fields associated with periods of strong magnetospheric convection, or mainly from induction electric fields associated with the occurrence of magnetospheric substorms [*Kamide et al*., 1998b].

Substorms are the most common form of disturbance in the Earth's magnetosphere. They are also the most visible disturbance at higher latitudes, manifesting themselves as bright and active polar aurora around local midnight. About 35 years ago, *Chapman* [1962] noted that substorms always accompany storms. In fact, he named them substorms because he thought of them as being the key elements of a magnetic storm.

In the picture drawn by *Chapman* [1962] and *Akasofu* [1968], substorms have the role of magnetic pumps, each of which inflates the inner magnetosphere with hot plasma. During the so-called substorm expansion, induction electric fields accelerate magnetospheric particles and inject them into the inner magnetosphere, where they become trapped and ultimately form the ring current. Magnetic storms occur when substorms deliver hot plasma to the inner magnetosphere faster than it can be dissipated.

The direct association between substorms and storms

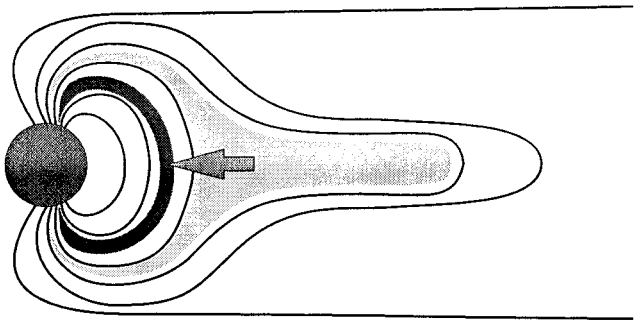

Figure 8. Compression of a flux tube on its way from the tail to the inner magnetosphere. Courtesy of M. Hesse.

was first questioned by at the end of the 1970s by *Kamide* [1979]. Thirteen years later, *Kamide* [1992] suggested that a magnetic storm develops as a result of a steady southward interplanetary magnetic field, rather than because of frequent intense substorms. The energy transfer mechanism from the solar wind to the magnetosphere for both storms and substorms is magnetic reconnection between the interplanetary magnetic field and the geomagnetic field, as was first suggested by *Dungey* [1961]. He noted that if the IMF were antiparallel to the geomagnetic field at the dayside magnetopause, the two fields would merge together: the magnetospheric and the interplanetary magnetic field lines should first cut and then reconnect with each other, leading to a transport of magnetic flux (and hence of energy) from the dayside to the nightside magnetosphere. According to its principle, reconnection is most efficient for southward IMF (since the magnetospheric field is northward), and it has been confirmed that steady and prolonged southward IMF is indeed a necessary prerequisite for intense storms [*Gonzalez et al*., 1994, and references therein]. However, whether steady southward IMF is only a necessary or also a sufficient condition, remained a much debated topic.

During the last 3 years, several studies have indicated that there is no causal relationship between substorms and storm time ring current development. Using a linear prediction technique, *McPherron* [1997] showed that a coupling function based solely on the IMF predicts three quarters of the variance of *Dst*. On the theoretical side, *Wolf et al*. [1997] presented results of the Rice convection model, a simulation model developed for treating the dynamics by which plasma moves from the tail into the magnetosphere, and reported that substorms have little effect on *Dst* compared with IMF-driven circulation.

A statistical study by *Iyemori and Rao* [1996] argued that the substorm expansive phase does not play a significant role in symmetric ring current generation and that it actually slightly weakens storms. However, *Rostoker et al*. [1997] showed that the data used by *Iyemori and Rao* [1996] were not adequate for conclusive remarks, and they suggested the need for a more thorough investigation of this issue. *Daglis et al*. [1999b] have argued that there is a significant influence of substorm occurrence on storm dynamics; they have shown that substorm signatures both in particle measurements in space and in ground magnetometers correlate well with changes in the *Dst* decrease rate.

In summary, substorms have been devalued from being the all-important component of a storm to being much less important. However, they are not a mere by-product of storms, but still play an important role in three distinct ways as described below.

4.1. Flow Unclogging

During a recent workshop at Kreuth, Germany, where a small group of space physicists discussed the causes and effects of magnetic storms [*Siscoe*, 1997], M. Hesse (personal communication, 1997) gave substorms a new role: substorms are earthquake-like releases of magnetic stresses that build up as strong magnetospheric circulation forces plasma from the magnetosphere's tail into the ring current. Hesse based his arguments on the so-called pressure catastrophe problem, which was first described by *Erickson and Wolf* [1980] and is sketched in Figure 8.

For the transport of plasma from the distant tail to the inner magnetosphere and into the ring current, there are two constraints. First, because the magnetospheric plasma is collision-free and hence resistance-free, plasma and magnetic field are frozen together as in a superconductor and move together with a bundle of field lines forming a flux tube filled with plasma. Second, if the transport is adiabatic, the temporal change of flux tube volume and pressure are related as $d(pV^{\gamma})/dt = 0$. Here $\gamma = 5/3$ is the adiabatic index, and the differential flux tube volume is related to the magnetic field strength B by the path integral along the field line $V = \int ds/B$.

Because of the $1/B$ dependence, a flux tube volume in the tail is very large, while it is comparatively small in the inner magnetosphere. Hence, as sketched in Figure 8, the volume of a flux tube decreases rather strongly on its way from the tail to the inner magnetosphere. Since pV^{γ} has to be kept constant, the pressure would increase even more dramatically. The massive buildup of plasma pressure should choke the flow and stop further circulation.

Substorms had long been suggested to be the process by which convection solves its pressure catastrophe problem. Hesse was the first to recognize that this suggestion identifies the role that substorms play in magnetic storms. As sketched in Figure 9, substorm-associated reconnection at a near-Earth neutral line will cut off the tailward part of the flux tube and thus strongly reduce the flux tube volume. Consequently, the flow will be unclogged and can proceed into the inner magnetosphere.

4.2. Recurrent Heating

Figure 10, from *Baumjohann et al*. [1996], shows that the average ion temperature in the near-Earth tail is

different around substorm onsets that occurred during the main phase of a magnetic storm from those that were not accompanied by magnetic storm activity. In both cases, the heating of the ion population in the central plasma sheet occurs during the substorm expansion phase. The temperature increase from substorm onset to the beginning of the recovery phase is about the same for both types of substorms, roughly 2 keV. The difference between storm time and nonstorm substorms lies in the average levels of the ion temperature before the onset, and thus also in the typical energy of the ion populations in the central plasma sheet during the expansion and recovery phases. In addition, the heating seems to occur more rapidly during storm time expansion phases, resulting in an average ion energy of 8 keV only 15–30 min after the onset of a storm time substorm. In contrast, a typical central plasma sheet ion has only 3–4 keV during the expansion phase of nonstorm substorms. That tail plasma is already quite energetic before the onset of a typical storm time substorm must be a result of previous substorm activity, which is much more likely to occur during magnetic storm activity due to the sustained southward interplanetary magnetic field and thus enhanced solar wind–magnetosphere coupling typical for the storm main phase.

Liu and Rostoker [1995] have shown that the tail plasma will gain energy during a series of substorms if it is recirculated back and forth between the tail and the inner magnetosphere. In an illustrative model sketched in Figure 11, *Liu and Rostoker* [1995] assumed for simplicity that one half of the energetic ions are field aligned (0° *pitch angle*), while the other half have a purely gyratory motion (90° pitch angle). During the growth phase, the field is stretched and gets weaker. Hence the ions will experience Fermi deceleration (0° particles), which is proportional to the square of the ratio of the lengths of the field lines before and after stretching, and betatron deceleration (90° particles), which is proportional to the ratio of the field strength before and after. In the highly stretched *current sheet* the energetic ions will behave nonadiabatically and undergo pitch angle scattering. In the illustrative model this process is mimicked by assuming that the two populations will switch their pitch angles, i.e., 90° → 0° and 0° → 90°. The subsequent *dipolarization* will accelerate the ions adiabatically by the Fermi and betatron process, since the field now becomes stronger and the field lines become shorter.

At first guess, one might think that there will be no

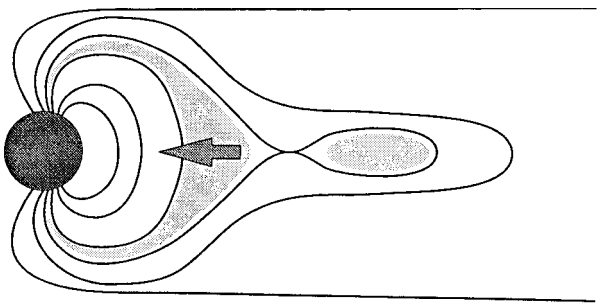

Figure 9. Diagram showing that magnetic reconnection effectively reduces the flux tube volume. Courtesy of M. Hesse.

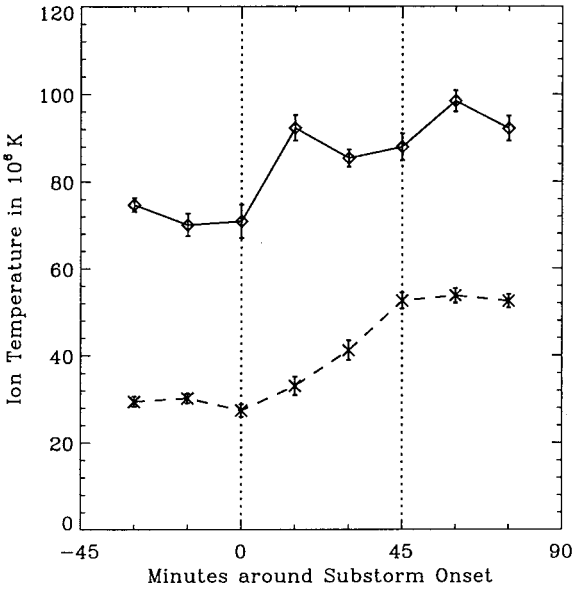

Figure 10. Average variation of the ion temperature in the central plasma sheet for substorms occurring during the main phase of a storm (solid line) and for nonstorm subaborms (dashed line). The radial range of the measurements was 10–19 R_E. From *Baumjohann et al.* [1996].

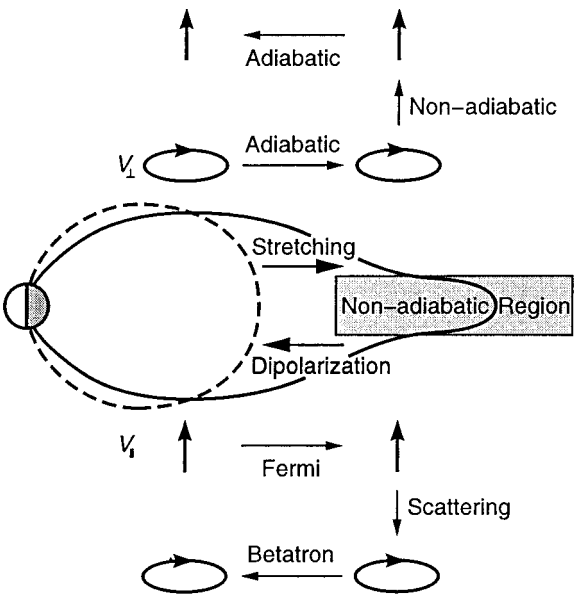

Figure 11. Schematic illustration of the nonadiabatic acceleration process during a substorm cycle. The stretching and dipolarization of the magnetic field are associated with the growth and expansion phase. In the highly stretched current sheet, keV ions become nonadiabatic and undergo pitch angle scattering.

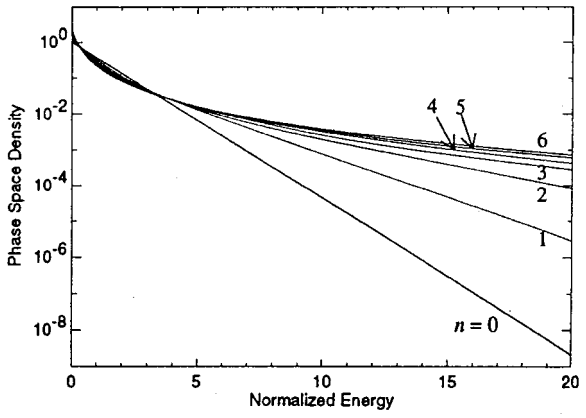

Figure 12. Evolution of a Maxwellian distribution into a kappa-like distribution due to subsequent (n = 1–6) recirculations [*Liu and Rostoker*, 1995].

net gain in energy during this process, and there would be none if there were no pitch angle scattering. Owing to the nonadiabatic scattering process, the Fermi-decelerated ions are betatron accelerated and vice versa. Assuming that one half of the particles, typically those starting with 0° pitch angle, experience an overall energy gain by a factor of λ, the energy of other half must decrease to 1/λ. Hence the average energy of a scattered particle after one substorm cycle is $W_1 = W_0(\lambda/2 + 1/2\lambda)$. Except for very peculiar magnetic field geometries with $\lambda = 1$, the energization coefficient, i.e., the factor enclosed by the parentheses, is always greater than unity.

Of course, the illustrative model is very simple and not very realistic. However, *Liu and Rostoker* [1995] also performed simulation runs, starting with Maxwellian distributions. Following a few subsequent recirculations, the distribution functions developed a high-energy tail. In the saturation limit, the suprathermal tail becomes so enhanced that the original Maxwellian are turned into a kappa distribution (see Figure 12).

4.3. Ionospheric Outflow

Substorms play an important role in terms of compositional changes in the ring current. The major compositional change is due to ionospheric outflow, which is strongly associated with substorms. Discrete enhancements of O^+ ions, which are the main signature of ionospheric outflow, have been observed by spacecraft in the inner magnetosphere during both growth and expansion phases of substorms [*Strangeway and Johnson*, 1983; *Baker et al*., 1985; *Möbius et al*., 1987; *Daglis et al*., 1991a, b, 1994, 1996; *Gazey et al*., 1996]. Ground-based radar observations, as well as observations in the upper ionosphere by polar-orbiting spacecraft, confirmed the association of strong ionospheric outflow (mainly O^+ ions) with substorm expansion [e.g., *Reiff et al*., 1988; *Wahlund and Opgenoorth*, 1989; *Wahlund et al*., 1992; *Gazey et al*., 1996].

At substorm onset the nightside magnetic field relaxes from the stretched configuration it obtains during the growth phase to a more dipole-like configuration [*McPherron*, 1972; *Kokubun and McPherron*, 1981; *Baker*, 1984]. This is due to a disruption or diversion or reduction of the near-Earth cross-tail current [*Kaufmann*, 1987; *Baker and McPherron*, 1990; *Lui et al*., 1992]. The magnetic field dipolarization is accompanied by strong induced electric fields [*Aggson and Heppner*, 1977; *Moore et al*., 1981; *Aggson et al*., 1983]. Such electric fields are very efficient in accelerating ionospheric outflowing O^+ ions [*Delcourt et al*., 1990b, 1991; *Wodnicka and Banaszkiewicz*, 1996, 1997], while they are less efficient for the energization of H^+ ions [*Fok et al*., 1996]. The reason for the preferential acceleration of O^+ ions is related to the breakdown of the *first adiabatic invariant* and to its dependence on particle mass [*Aggson and Heppner*, 1977; *Delcourt et al*., 1990b]. This is further supported by the fact that results of studies assuming adiabaticity [e.g., *Mauk*, 1986; *Lewis et al*., 1990] are incompatible with the actual energy spectra observed during substorms [e.g., *Kistler et al*., 1990].

Aggson and Heppner [1977] showed that the large, transient, induced electric fields observed in the inner magnetosphere cause violation of the second and third adiabatic invariants for H^+, and violation of all three adiabatic invariants for heavier ions. *Delcourt et al*. [1990b] performed detailed simulations and showed that O^+ ions with initial energies of 100 eV may reach energies of >100 keV, depending on initial latitude, while H^+ ions with the same initial energies are limited to final energies of <20 keV. Hence, depending on the effective ionospheric source geometry and transport paths, outflowing ionospheric O^+ ions can attain very high energies and become a significant, and occasionally dominant, component of the ring current. This should be expected during intense storms, which are always accompanied by frequent, intense substorms [e.g., *Kamide*, 1992] and thus large induced electric fields.

Some of the effects of O^+ abundance enhancements are discussed in section 3.2.3. An interesting implication of O^+ enhancements, regarding the evolution of magnetic storms, should be mentioned here. *Rothwell et al*. [1988] predicted that a higher concentration of O^+ in the nightside magnetosphere will permit substorm breakup at lower L values. This process is related to an earlier storm study by *Konradi et al*. [1976], which showed that the substorm injection boundary was displaced earthward with each successive substorm during the magnetic storm. During a series of substorms the ionospheric feeding of the magnetosphere is most effective [*Daglis and Axford*, 1996], both in quantity and in spatial extent. Intense O^+ outflows, associated with successive intense substorms, which are always observed during large storms, may thus facilitate successive inward penetration of ion injections. The result would be the trapping of more energetic ions, resulting in a stronger ring current and thus larger *Dst* depression.

An O^+ influence on the localization of substorm onset was also proposed by *Baker et al*. [1985]. The scenario of progressively earthward and duskward [*Baker et al*., 1985] substorm onsets and accompanying ion injections during storm time substorms can be investigated only through coordinated multipoint measurements [*Daglis et al*., 1995; *Lockwood*, 1997] or through neutral atom imaging of the inner magnetosphere [*Roelof*, 1989; *Williams et al*., 1992; *Daglis and Livi*, 1995]. Neutral atom imaging of the ring current is discussed in the following section.

5. RING CURRENT DECAY THROUGH CHARGE EXCHANGE LOSSES

The main mechanism of ring current decay is charge exchange of the ring current ions with the geocorona. The geocorona is an exospheric extension of relatively cold (~1000 K) neutral atoms, which resonantly scatter solar Lyman α radiation [*Chamberlain*, 1963]. Since oxygen atoms must have an energy of ~10 eV to overcome the Earth's gravitational field, while lighter atoms and molecules need much less energy to escape, the geocorona is essentially hydrogen gas. The geocoronal density falls off quickly with radial distance, so that at altitudes of $\geq 10\ R_E$, collisions between ions and geocoronal hydrogen are rare. At the ring current altitudes, however, such collisions are frequent enough to account for significant loss of ring current ions.

The importance of this process for the loss of magnetospheric plasma was considered ~40 years ago. *Stuart* [1959] pointed out that charge exchange between H^+ and atmospheric hydrogen atoms can very effectively remove energetic H^+ trapped by the geomagnetic field. In the same year, *Dessler and Parker* [1959], motivated by laboratory results of *Fite et al*. [1958], suggested charge exchange between energetic ions and neutral exospheric hydrogen to be an effective means of ring current decay. Through this process, energetic ions colliding with neutral exospheric gas may acquire an electron from the cold neutral atom and become neutralized. In the case of energetic H^+, charge exchange generates an energetic neutral hydrogen atom, which escapes magnetic field trapping and follows a ballistic orbit with essentially the same energy and direction of the incident H^+.

5.1. Charge Exchange Processes

The main charge exchange losses of ring current ions are due to interactions with cold exospheric hydrogen:

$$H^+ + H \rightarrow H + H^+$$

$$O^+ + H \rightarrow O + H^+$$

$$He^{++} + H \rightarrow He^+ + H^+$$

$$He^+ + H \rightarrow He + H^+$$

Since the geocorona is essentially a cold hydrogen gas, the above processes are the main ones causing substantial ring current losses. Ions mirroring off the equatorial plane (that is, ions with small equatorial pitch angles), reach relatively low altitudes and are subject to additional charge exchange with oxygen atoms in the upper atmosphere:

$$H^+ + O \rightarrow H + O^+$$

$$O^+ + O \rightarrow O + O^+$$

$$He^{++} + O \rightarrow He^+ + O^+$$

$$He^+ + O \rightarrow He + O^+$$

Spjeldvik and Fritz [1978] suggested the following general formulation of charge exchange loss reactions:

$$Y^{p+} + X \rightarrow Y^{q+} + X^{s+}, \tag{8}$$

where X denotes cold exospheric atoms and Y denotes energetic ions with nucleonic charge number M and charge p, while $p = q + s$ and $0 \leq q < p \leq M$.

The main parameters involved in the calculation of the charge exchange lifetime of energetic ions are the neutral atomic hydrogen or oxygen density, the charge exchange cross section of the ions, and the equatorial pitch angle of the ions. The neutral hydrogen geocoronal density radial profile has been calculated by *Rairden et al*. [1986] using observations of geocoronal emission of scattered solar Lyman α radiation from the ultraviolet photometer on Dynamics Explorer 1 over the time period 1981–1985. The data were fit to a spherically symmetric isothermal (1024 K) Chamberlain model. *Chamberlain* [1963] introduced a comprehensive theory for the planetary exospheric regions, where collisions are rare and the controlling factors are gravitational attraction and thermal energy. In the Chamberlain model the theoretical profiles of the hydrogen density versus altitude are given as a function of temperature. Alternatively, the hydrogen density profile versus altitude can be derived by means of an extensive empirical thermospheric model, known as MSIS [*Hedin*, 1987], which is based on in situ mass spectrometer and incoherent radar scatter data. This model incorporates data from several satellites, including Dynamic Explorer, and numerous rocket probes.

Cross sections for several charge exchange processes between ions and neutral atoms have been obtained through laboratory measurements; most relevant publications were listed recently by *De Michelis and Orsini* [1997] and by *Noël* [1997b]. Unfortunately, the charge exchange cross sections of several geophysically interesting ions are not yet known, either because the laboratory measurements did not cover the proper energy range or because the target gas did not correspond to the exospheric gas [*Spjeldvik and Fritz*, 1978]. Because charge exchange cross sections are energy and species (mass) dependent, there are large differences among charge

exchange lifetimes of the various ring current ion species (see also Figure 7). Therefore compositional changes in the ring current critically influence ring current decay due to charge exchange, as was already pointed out in section 3.2.3. Charge exchange lifetimes also have a strong dependence on ion location because neutral hydrogen density falls off quickly with altitude [*Rairden et al*., 1986]. Therefore decay of the innermost ring current is the fastest.

The mean lifetime of any energetic ion confined to the equatorial plane for charge exchange decay with geocoronal hydrogen is

$$\tau_e = 1/[n(r_0)\sigma v] \tag{9}$$

where $n(r_0)$ is the neutral hydrogen density in the equatorial plane (dependent on distance from the Earth), σ is the charge exchange cross section of the ion (energy and mass dependent), and v is the velocity of the ions [*Smith and Bewtra*, 1978]. The relationship between the lifetime τ_m of a particle mirroring off the geomagnetic equator at a mirror latitude λ_m and the lifetime τ_e of (the same) particle confined to the equator is

$$\tau_m = \tau_e \cos^{\gamma} \lambda_m \tag{10}$$

Smith and Bewtra [1976] and *Cowley* [1977] found independently by numerical evaluation that for the typical ring current altitudes, $\gamma \simeq 3$–4.

5.2. Role of Charge Exchange in the Modeling of Ring Current Decay

Ring current decay is due mainly to charge exchange with exospheric neutrals, Coulomb collisions with thermal plasma, and wave-particle interactions. Since neutralized ring current particles are able to escape the inner magnetosphere trapping region, charge exchange acts as a major direct loss mechanism for the ring current and has to be considered carefully in any ring current decay modeling. *Sheldon and Hamilton* [1993] showed that charge exchange losses are most important for singly charged ions (H^+, O^+) with energies of up to a few hundred keV. At higher energies the charge exchange cross sections decrease, and losses due to wave-particle interactions become increasingly important, especially for energetic protons. For example, the cross section for charge exchange between cold hydrogen and 100 keV protons is 2 orders of magnitude smaller than the corresponding cross section for 10 keV protons [*Smith and Bewtra*, 1978].

Ions with higher charge states, such as He^{++} or O^{++}, have to undergo multiple charge exchange with the exospheric gas before they can escape. A by-product of He^{++} charge exchange is He^+; He^+ due to He^{++} charge exchange is thought to make a significant (if not dominant) part of the total magnetospheric He^+ population [*Kremser et al*., 1993].

Cladis and Francis [1985] were the first to quantitatively include charge exchange of H^+ and O^+ with their neutral counterparts in a ring current decay model. Recently, several large-scale models of ring current decay have incorporated the effects of charge exchange [e.g., *Fok et al*., 1995, 1996; *Jordanova et al*., 1994; *Noël*, 1997b]. Use of ring current measurements allowed testing and improvement of the models in order to match the actual observations. The extensive measurements of the CHEM spectrometer on board the AMPTE/CCE spacecraft (see section 3.1), provided new information on the bulk of the ring current under storm conditions as well as under quiet conditions [e.g., *Gloeckler and Hamilton*, 1987; *Hamilton et al*., 1988; *Lui and Hamilton*, 1992]. These measurements were used in a number of ring current evolution investigations [*Kistler et al*., 1989; *Sheldon and Hamilton*, 1993; *Chen et al*., 1994; *Jordanova et al*., 1994; *Fok et al*., 1995, 1996; *Orsini et al*., 1994; *Milillo et al*., 1996a, b].

Fok et al. [1995] developed a ring current decay model considering charge exchange with neutral hydrogen and *Coulomb collisions* with the plasmasphere. Unlike previous ring current models [e.g., *Kistler et al*., 1989; *Sheldon and Hamilton*, 1993; *Chen et al*., 1994], their model was not restricted to equatorially mirroring particles; they considered ring current ions of all pitch angles and reduced the three-dimensional problem to two dimensions by bounce averaging the kinetic equation of phase space density. The approach is valid, since the bounce periods of ring current ions are typically much shorter than their charge exchange and Coulomb decay lifetimes. *Fok et al*. [1995] compared the results of their model with AMPTE/CCE CHEM measurements of the ring current during the great storm of February 1986. The model generally reproduced the measured fluxes of the three major ring current ion species H^+, O^+, and He^+. However, the calculations overestimated the H^+ fluxes at energies above 100 keV. Fok et al. suggested that wave-particle interactions are responsible for this discrepancy (see section 6).

Jordanova et al. [1996a] investigated the modification of the ring current ion distributions caused by energy degradation, pitch angle scattering, and charge exchange. The changes in the distribution functions of the ring current H^+ and O^+ ions were analyzed considering each loss effect. *Jordanova et al*. [1996a] found that the loss of O^+ ions proceeds at a much slower rate, so that the modification of their distribution functions becomes significant only after 32 hours. Change exchange is the most important loss process (especially for H^+), but Coulomb collisions are not negligible at lower energies (<10 keV), especially for heavier ions. The Coulomb energy degradation process builds up a low-energy heavier ion population (first shown by *Fok et al*. [1993]); when all loss mechanisms are included, the heavier ion flux increases at low energies (~1–5 keV), while it decreases at higher energies. It was also shown that Coulomb pitch angle diffusion scatters ions into the *loss cone*, thus increasing precipitation at low energies and at low L shells. From the previous considerations it follows

that during the storm recovery phase the high-energy part (>10 keV) of the ring current distribution is dominated by H^+ ions, while heavier ions dominate the lower energy range.

5.3. Energetic Neutral Atoms: Remote Sensing of the Ring Current

Energetic neutral atoms (*ENA*) are the product of charge exchange between singly charged energetic ions and the cold neutral hydrogen of the geocorona (Figure 13). The energy distributions of the ENA depend on the ion energy distributions and on the cross sections of the relevant charge exchange interactions. In the case of energetic neutral hydrogen and oxygen (products of H^+ and O^+ charge exchange), the energy distributions span the range between a few eV and a few hundred keV. Energetic neutral atoms are not affected by magnetic or electric field forces and therefore leave the interaction region in ballistic orbits, with essentially the energy and direction of the incident ion. Hence the geocorona acts like an imaging screen for the ring current. Remote sensing of ENA provides line-of-sight integrated observations of the source populations [e.g., *Roelof*, 1989].

The existence of ENA was discovered in 1951 when a blue-shifted H α line (due to precipitating energetic neutral hydrogen) was detected during an auroral display [*Meinel*, 1951]. *Dessler and Parker* [1959] were the first to suggest charge exchange as an efficient means of ring current decay. *Moritz* [1972] reported detection of energetic (>250 keV) protons at equatorial low altitudes (<600 km) and suggested that they were protons from the outer radiation belt that became neutral by charge-exchange, reached low altitudes, and then reionized just before detection. Particle transport between the ring current and the upper atmosphere due to charge exchange has further been invoked to explain the appearance of midlatitude and low-latitude aurora [*Tinsley*, 1981] and the heating of the *thermosphere* at these latitudes [*Ishimoto et al*., 1986].

The first clear evidence of ENA generation in the Earth's magnetosphere came from ion detectors onboard the IMP 7, IMP 8, and ISEE 1 spacecraft. It was shown that energetic particles were observed coming from the direction of the Earth [*Hovestadt and Scholer*, 1976; *Roelof et al*., 1985] when the spacecraft were located out of the magnetosphere. *Roelof* [1987] extended these observations to obtain the first-ever global image of the ring current, by iterating model ring current distributions in a dipole magnetic field until their convolution through charge exchange with the model geocorona reproduced the actually observed ENA patterns.

5.3.1. Recent observations and modeling. After the first reports in the 1970s and 1980s, no more ENA observations were reported for a long time. However, in recent years the design and development of space instrumentation suitable for ENA detection became a crucial task for many experimenters [*Pfaff et al*., 1998]. Recently, sporadic ENA observations have been reported,

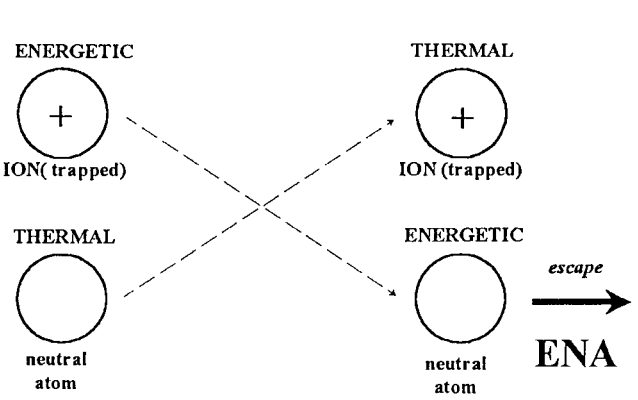

Figure 13. Schematics of the charge exchange process.

from both high-altitude and low-altitude spacecraft. Two instruments on board the Geotail spacecraft have been the first to experimentally confirm the feasibility of ENA observations. *Lui et al*. [1996] reported the first composition measurements of ENAs, made by the EPIC ion spectrometer during a magnetic storm on October 29–30, 1994, when Geotail was located at a geocentric distance of ~14 R_E, viewing the dayside magnetosphere. The measured particles could be identified as ENAs because the direction of their flux steadily tracked the direction of the Earth and was uncorrelated with the changing orientation of the ambient magnetic field. The observations yielded the storm time evolution of ENA fluxes of hydrogen, helium, and oxygen separately, as well as their energy spectra. ENA fluxes and the recovery rate of the *Dst* index were roughly steady, consistent with charge exchange being an important loss process for the storm time ring current. For energies of >200 keV, the intensity of energetic oxygen was the highest, consistent with the relatively short charge-exchange lifetime of energetic O^+ (see section 3.2.3 and Figure 7).

Wilken et al. [1997] reported ENA measurements by the HEP-LD energetic particle spectrometer, on board Geotail. HEP-LD is the first instrument that can discriminate between ENAs and charged particles in the energy range 77–200 keV, when it is operated in the ENA mode. ENA fluxes were measured on October 18, 1992, while Geotail was located at dusk, at a geocentric distance of ~12 R_E, traveling tailward. HEP-LD operated in the ENA mode for about 3 hours and detected a relatively low ENA flux, consistent with the low geomagnetic activity ($Kp = 1+$).

More recently, very encouraging ENA observations have been made by the POLAR spacecraft. Owing to the favorable polar orbit that brings the POLAR spacecraft out of the terrestrial magnetosphere regularly, the CEPPAD-IPS experiment on board POLAR has obtained prolific ENA measurements. *Henderson et al*. [1997] presented the first ENA images from POLAR, for two storms in August and October 1996. The measurements show the expected enhancement of ENAs arising from

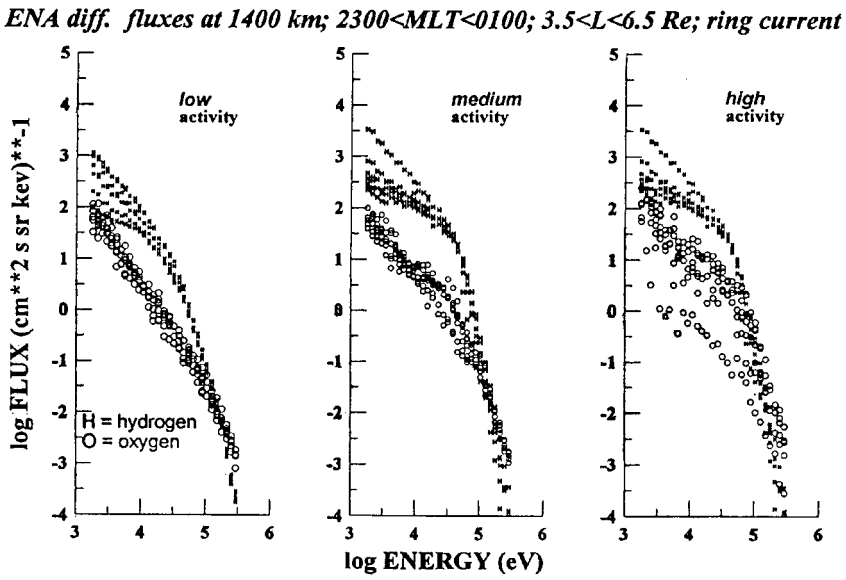

Figure 14. Plots of simulated H and O ENA differential fluxes as a function of energy. The observation point altitude is 1400 km, and the look direction is on the GSM X–Y plane, with magnetic local time (MLT) ranging between 2300 and 0100. Three geomagnetic activity levels are considered: low ($AE < 500$ nT), medium (500 nT $< AE <$ 1000 nT), and high ($AE >$ 1000 nT) [*Orsini et al.*, 1994, Figure 8].

the buildup of the storm-time ring current. Although the images obtained by CEPPAD are rather coarse, they nevertheless are a verification of the potential of ENA imaging. Furthermore, a first attempt to relate the ENA emission detected by CEPPAD-IPS with the ring-current *Dst* index has been published by *Jorgensen et al.* [1997].

In addition to the possibility of neutral atom imaging the ring current from high altitudes (i.e., out of the magnetosphere), *Orsini et al.* [1994] showed the feasibility of ENA imaging from low-altitude vantage points. The limit for realistic measurements is at ~400–500 km: below this limit, ENA increasingly interact with exospheric neutral particles, so that the source ion energy and direction information is lost [*De Michelis and Orsini*, 1997]. Low-altitude ENA imaging has to face the problem of discriminating the ENA signal from energetic ion signatures expected at these altitudes. However, ENA imaging from low-altitude vantage points can provide essential information complementary to what can be obtained from high altitude ENA imaging. For instance, focused imaging of specific regions is feasible. An additional advantage is that secondary ENA originating from interactions of primary ENA with atoms in the upper atmosphere (i.e., below the vantage point), do not contaminate measurements (as in the case of high-altitude ENA imaging), since they do not mix with the primary ENA originating in the ring current.

The expected fluxes of precipitating ENA at low altitudes have been realistically simulated by using AMPTE/CCE-CHEM energetic ion measurements as the input source population [*Orsini et al.*, 1994; *Milillo et al.*, 1996a, b]. During quiet periods the estimated energetic neutral hydrogen fluxes originating from the geomagnetic equatorial plane and integrated between 3 and 9 R_E geocentric distance, vary between 5×10^2 and 10^{-2} [1 cm^{-2} s^{-1} sr^{-1} keV^{-1}] at 5 keV and 120 keV, respectively (Figure 14). The estimated energetic neutral oxygen fluxes are somewhat lower than the hydrogen fluxes at low energies, which is expected since the quiet time ring current O^+ flux is low compared that of H^+. However they overlap the energetic hydrogen fluxes at energies >80 keV. This is an expected effect of the differences in the charge exchange cross sections (which are energy and species dependent) and has been verified through the ENA observations reported by *Lui et al.* [1996].

PIPPI, the first instrument designed to exclusively measure ENAs, flew on board the Swedish satellite ASTRID on a low-altitude (1000 km) polar orbit. The instrument was operational during the first 5 weeks of the mission and measured ENAs in the energy range 13–140 keV. The available data demonstrate the advantages of ENA imaging from a low-altitude/high-latitude orbit. Ring current ions on a given L shell encounter a denser exosphere at high latitudes, so that the ENA emission is stronger at higher than lower latitudes. ENA images presented in a fish eye projection clearly show dawn-dusk flux asymmetries during geomagnetically active periods [*Barabash et al.*, 1997; *Brandt et al.*, 1997].

However, as was already mentioned, ENA imaging provides line-of-sight integrated observations of the ring current ion population. An unfolding of the product $j_{\text{ion}} n_{\text{H}}$ (where j_{ion} is the ion flux and n_{H} is the geocoronal H density) from the line-of-sight integrals is required in order to extract physical parameters from the ENA images [*Daglis and Livi*, 1995]. The deconvolution can be done on the basis of an iterative comparison of the actual images with model images until the differences are minimized. The model images are simulated by convolving the neutral atom imaging instrument response with the neutral atom emission as computed from parametric models of the ion distributions [*Roelof*, 1987]. Furthermore, *Roelof et al.* [1993] proposed the use

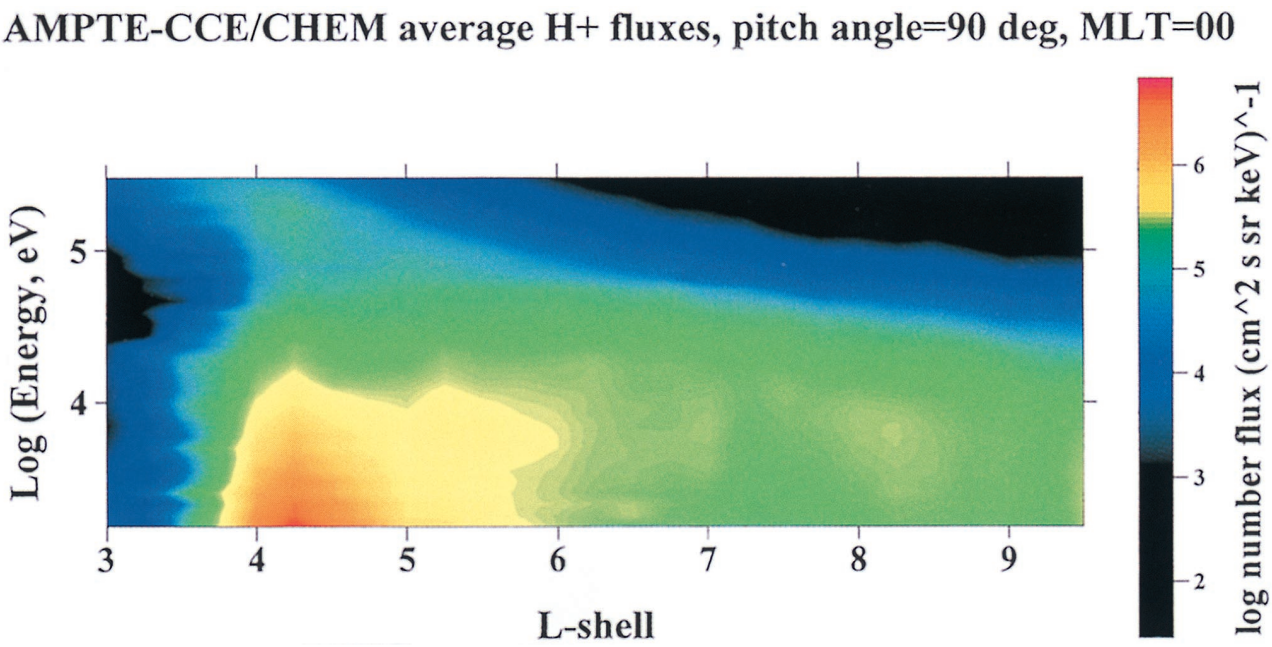

Plate 1. Color-coded H^+ differential fluxes as a function of energy and L shell, as measured by the AMPTE/CCE CHEM experiment and averaged over the whole mission time period (adapted from *Orsini et al*. [1994]). The fluxes at 0000 MLT for low geomagnetic activity ($AE < 100$ nT) are shown.

of empirical models of ion distributions to serve as the basis of comparison with ENA image simulations. For the purpose of constructing comparison images, large databases of in situ measured ring current ion distributions are valuable. Such databases can also be very useful as an a priori information of gross local characteristics. The AMPTE/CCE-CHEM measurements permitted the construction of such a database, which has been successfully used for ENA-related simulation studies [*Orsini et al*., 1994; *Milillo et al*., 1996a, b, in press, 1998]. The mission-averaged AMPTE/CCE-CHEM measured ring current ion distributions were organized as a function of distance, local time, pitch angle and geomagnetic activity by *Orsini et al*. [1994]. Plate 1 shows an example of the H^+ distributions for 2400 magnetic local time (MLT) at low geomagnetic activity.

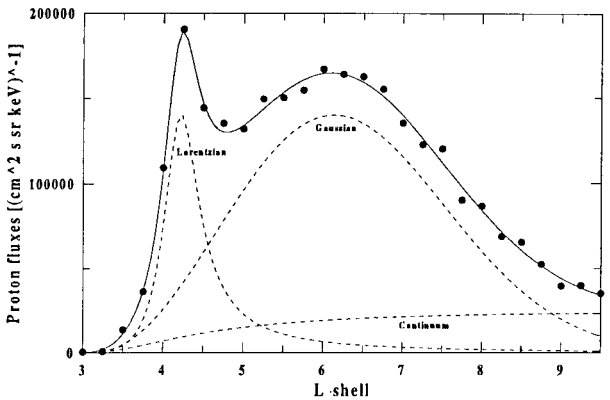

Figure 15. Average H^+ flux as a function of L shell for E = 32.4 keV at 2400 MLT, according to AMPTE/CCE CHEM measurements (dots) and the analytical function (solid line) of *Milillo et al*. [1998]. The three parts of the function are also plotted: the Lorentzian, the Gaussian, and the continuum. The agreement between the function and the AMPTE/CCE data is quite satisfactory [*Milillo et al*., 1998, Figure 1].

General analytical functions empirically describing the ion distributions in the inner magnetosphere would also be valuable tools for ENA simulations. Recognizing this, *Milillo et al*. [in press, 1998] have recently used the AMPTE/CCE-CHEM ion database of *Orsini et al*. [1994] to derive a multi-parametric analytical function, which can describe the equatorial ring current ion fluxes. The analytical function is a combination of a Lorentzian, a Gaussian and a continuum (Figure 15). The first applications of the function have been very encouraging. In Figure 16 the ENA fluxes generated by the ring current protons, observed from a low altitude vantage point located at 2400 MLT, are simulated by using the AMPTE/CCE-CHEM database (dots) and the function (continuous line) respectively.

A "by-product" of ENA imaging, which however can be of great benefit to ring current research and to magnetospheric research in general, is the chance to instantaneously estimate the large-scale convection electric field. *Milillo et al*. [1996b] pointed out this possibility, which is based on the properties of ring current ions moving along equipotential surfaces under conservation of the first and *second adiabatic invariants* [*Whipple*, 1978]. A consequence of the ion motion is an adiabatic heating towards dusk, and an adiabatic cooling towards dawn. The ENAs generated from the ring current ions through charge exchange should also exhibit this dawn-

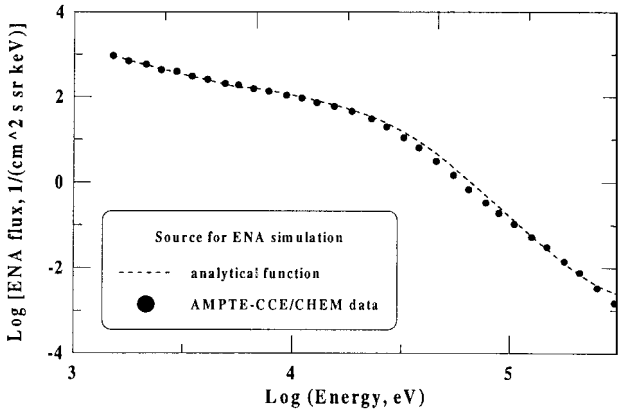

Figure 16. Simulated energy distribution of energetic neutral hydrogen, at a low-altitude vantage point at 2400 MLT. Dots refer to simulations using AMPTE/CCE CHEM measurements as the source distributions of the ENA flux, while the dashed line shows the simulated ENA spectrum resulting from the use of the analytical function derived by *Milillo et al.* [1998]. Reprinted with permission from Elsevier Science.

dusk asymmetry. *Orsini et al.* [1998] used the AMPTE/CCE-CHEM ion database to simulate ENA spectra in the dawn and dusk sectors of the nightside magnetosphere and to derive through the analytical function of *Milillo et al.* [1998] the cross-tail potential (Figure 17). Their estimation (19 kV) is in good agreement with the value calculated by *Whipple* [1978] (20 kV) at a geocentric distance of 4 R_E. An ENA-based estimate of the convection electric field could be obtained with a time resolution of an ENA instrument duty cycle, that is, just a few minutes. A continuous monitoring of the convection electric field, which is of prime importance for the formation of the ring current, with such a time resolution is clearly of high merit to ring current and storm/substorm research.

6. WAVE-PARTICLE INTERACTIONS IN THE RING CURRENT

Although classical collisional processes provide the dominant loss process for ring current ions, there is compelling evidence that pitch angle diffusion by plasma waves also contributes to ion loss, especially during the main phase of a storm. Large-scale models incorporating the effects of charge exchange and Coulomb scattering [e.g., *Fok et al.*, 1995] tend to overestimate the flux of protons above tens of keV. Furthermore, they yield a pitch angle distribution that is too flat for energies >100 keV. Additional pitch angle scattering by plasma waves has been suggested as a mechanism to account for these discrepancies [*Fok et al.*, 1996]. Intense plasma waves also provide an efficient process for energy transfer between different components of the plasma. Waves are particularly important as a heating mechanism for thermal heavy ions [e.g., *Gendrin and Roux*, 1980; *Mauk*, 1982; *Anderson and Fuselier*, 1994; *Horne and Thorne*, 1997], and they can also transfer energy from ring current H^+ to O^+ during magnetic storms [*Thorne and Horne*, 1994, 1997].

At least two distinct classes of plasma waves are able to interact with ring current ions. The most widely studied interactions involve electromagnetic ion cyclotron (EMIC) waves. The timescales for scattering of ions into the loss cone during resonant interactions with EMIC waves can be rapid [*Lyons and Thorne*, 1972]. This is attractive because studies of the ring current energy balance [*Gonzalez et al.*, 1989; *Prigancová and Feldstein*, 1992] suggest that energy loss timescales during the main phases of intense-to-great geomagnetic storms may reach values as low as 0.5–1.0 hours, far too rapid to be the result of charge exchange or Coulomb collision processes. *Feldstein et al.* [1994] report decay times for the asymmetric component of the ring current with values of the order of an hour in the dusk to noon MLT sector.

6.1. Magnetosonic (Oblique Whistler Mode) Waves

Although scattering of ring current ions by EMIC waves is thought to be predominant, *magnetosonic* (oblique *whistler mode*) *waves* can also resonate with ring current ions and contribute to the net rate of particle loss. Low-frequency electromagnetic emissions between the proton gyrofrequency and the *lower hybrid frequency* are frequently observed near the magnetic equatorial plane [*Russell et al.*, 1970; *Gurnett*, 1976; *Laakso et al.*, 1990]. These waves, which occur in the magnetosonic (oblique whistler) branch, can be excited by ion ring distributions [*Perreaut*, 1982; *Boardsen et al.*, 1992] that develop in the ring current in association with convective injection events. Wave growth peaks at highly oblique angles of propagation in harmonic frequency bands associated with multiple harmonics of the proton gyrofrequency. The waves are observed over a broad range of L both inside and outside the *plasmapause*. Broadband whistler mode hiss (also called plasmaspheric hiss) is

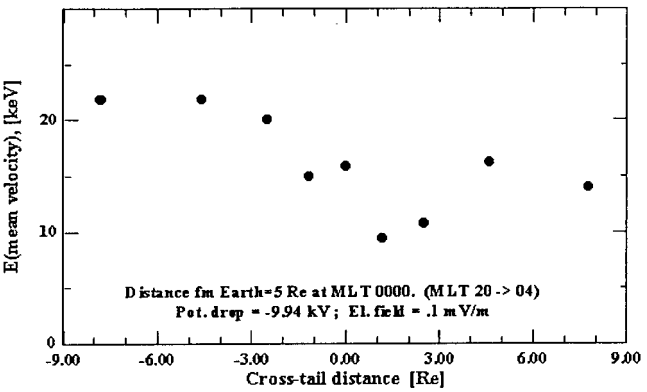

Figure 17. Profile of the quantity $E_c = 0.5mv^2$ as a function of the distance from the local midnight meridian at $x = 5\ R_E$ from Earth. Reprinted from *Orsini et al.* [1998] with kind permission from Kluwer Academic Publishers.

also present continuously throughout the plasmasphere [*Thorne et al*., 1973]. The intensity of plasmaspheric hiss is enhanced during the recovery phase of magnetic storms [*Smith et al*., 1974]. For oblique angles of propagation, both magnetosonic waves and plasmaspheric hiss can interact with ring current ions ($E \geq 10$ keV). *Kozyra et al*. [1994, 1995] have performed detailed calculations of the rate of ion scattering by such waves using the methodology described by *Lyons* [1974]. They conclude that the diffusion timescales are in the range of 1–100 days. These timescales are competitive with the loss time associated with charge exchange and Coulomb drag [*Fok et al*., 1991] for ion energies above ~80 keV. This suggests that such waves could play an important role in the long-term evolution of the more energetic components of the ring current.

6.2. EMIC Waves

Observations by the AMPTE/CCE spacecraft indicate that EMIC waves occur most frequently in the outer magnetosphere beyond $L = 7$ [*Anderson et al*., 1990, 1992a, b]. The wave spectral properties have a pronounced dependence on magnetic local time. Events occurring between 0300 and 0900 MLT have an average occurrence frequency of 3–4%. They have essentially *linear polarization* at all latitudes and are generally confined to the frequency band above the helium gyrofrequency Ω_{He^+}. Typically, the normalized wave frequency may extend up to $\omega/\Omega_{He^+} \simeq 2.5$–3.0. Events between 1000 and 1800 MLT have a much higher occurrence frequency (10–20%) and the waves generally occur in two distinct frequency bands separated by a noticeable spectral gap near Ω_{He^+}. The waves usually exhibit *left-hand polarization* near the equator and linear polarization at higher latitudes. The observed wave characteristics in the outer magnetosphere can be explained [*Horne and Thorne*, 1993, 1994] by realistic variations in key plasma parameters such as the thermal plasma density, helium composition, and the density and temperature anisotropy of energetic ring current protons.

During geomagnetic storms the source of free energy for wave excitation is greatly enhanced, and the optimum region for EMIC wave growth occurs at lower L shells along the duskside plasmapause [e.g., *Jordanova et al*., 1997; *Kozyra et al*., 1997]. Such waves can interact strongly with the bulk of the ring current ion population. The observed thermal anisotropy ($T_\perp > T_\parallel$) of ring current H^+ ions provides an adequate source of free energy for EMIC wave excitation. H^+ distributions, unstable to the amplification of ion cyclotron waves, are produced naturally in the inner magnetosphere through *betatron acceleration* of ions moving along adiabatic drift paths [cf., *Cornwall et al*., 1970]. The enhanced charge exchange loss of ring current ions with small pitch angles [*Cornwall*, 1977] deepens the loss cone and increases the anisotropy of the drifting ion distributions making them even more unstable to the generation of plasma waves. Theoretical studies of EMIC wave excitation have mainly concentrated on convective instabilities [*Kennel and Petschek*, 1966; *Perreaut et al*., 1976; *Gomberoff and Neira*, 1983; *Gendrin et al*., 1984; *Kozyra et al*., 1984; *Ludlow*, 1989; *Horne and Thorne*, 1993], in which the waves propagate with finite group velocity through the medium. However, conditions in the outer magnetosphere where the *plasma beta* is high, and where the energetic ion anisotropy ($A_{H^+} = T_\perp/T_\parallel - 1$) can be enhanced by solar wind compression [*Anderson and Hamilton*, 1993; *Ishida et al*., 1987], may permit the onset of absolute or nonconvective instabilities [*Wandzura and Coroniti*, 1975], in which the wave group velocity becomes essentially zero and waves can be amplified locally to large amplitude. *Roux et al*. [1982] considered the importance of nonconvective instabilities for interpreting EMIC waves observed by GEOS 1 and 2 near geostationary orbit and pointed out that inhomogeneities in the medium would probably prevent absolute instabilities from forming.

Rauch and Roux [1982] found that there is a class of waves above Ω_{He^+} that reflect at high latitudes and are geomagnetically trapped. Since the single transit gain may be small, *Roux et al*. [1982] suggested that such waves may be amplified each time they cross the magnetic equator, causing a laser-like growth to observable limits. Using the HOTRAY code, *Horne and Thorne* [1993] demonstrated that unless special density gradients exist (e.g., near the plasmapause), the laser-like effects cannot occur in the outer magnetosphere since the waves return to the favored equatorial growth region with large *wave normal angles*. Wave growth to observable levels must therefore occur on the first equatorial pass.

An example of the path integrated gain of EMIC in the outer magnetosphere ($L = 9$) is shown in Figure 18. The result was obtained using the HOTRAY code [*Horne and Thorne*, 1997] with plasma parameters based on AMPTE observations [*Anderson and Fuselier*, 1994; *Anderson et al*., 1996]. All waves are launched from below the magnetic equator so that on crossing the equator, the wave propagation vector **k** is approximately field aligned ($\psi = 0°$) and maximum gain is obtained. The rays are launched in the guided mode, and consequently, the ray paths follow closely the $L = 9$ field line. All rays are stopped before reflecting in the Northern Hemisphere at a location where $\omega < \omega_{bi}$ (ω_{bi} is the *bi-ion frequency*). The maximum path integrated gain is more than 60 dB, or 6 orders of magnitude in power, above the background noise level. Since the observed maximum power spectral density [*Anderson and Fuselier*, 1994] is typically only 3.5 orders of magnitude larger than that in the spectral slot region at $\omega \approx \Omega_{He^+}$, the calculated gain should be sufficient to produce observable waves.

To study the influence of EMIC waves on the evolution of the storm time ring current, global information is required on the density and composition of the thermal plasma and the distribution function of each energetic ion species. Wave propagation characteristics are con-

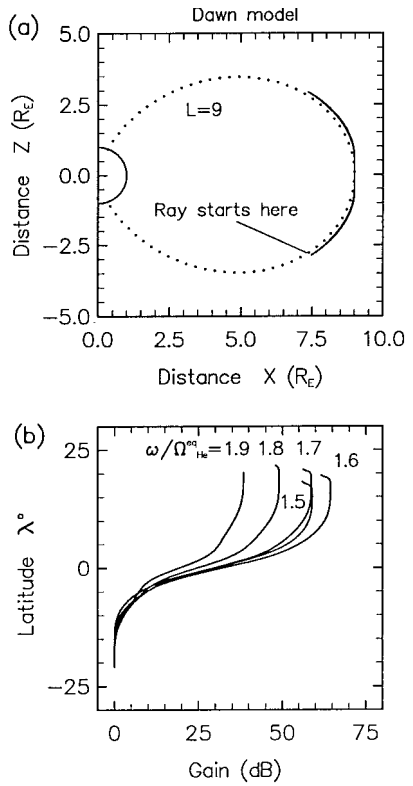

Figure 18. (a) Ray paths and (b) path-integrated gain for guided mode waves launched from below the magnetic equator in a dipole field using the HOTRAY code [*Horne and Thorne*, 1997]. The ray paths are calculated for dawn conditions with $N_e = 5 \times 10^6$ m^{-3} and $N_{He^+} = 5 \times 10^4$ m^{-3}. The dotted line corresponds to $L = 9$. Reprinted from *Orsini et al.* [1998] with kind permission from Kluwer Academic Publishers.

trolled by the thermal plasma, while the rate of wave growth or damping is a sensitive function of the distribution function of the energetic ring current population. Satellite observations can be utilized to assess the importance of wave growth at selected locations [*Anderson et al.*, 1996], but this information is unavailable on a global scale. Consequently, a realistic assessment of the potential for wave excitation and the overall affect of such waves on the ring current population requires a global numerical simulation.

The challenge in modeling wave-particle interactions on a global scale is the need to represent wave growth and particle diffusion self-consistently and to relate wave convective gains [*Horne and Thorne*, 1994] to resultant wave amplitudes. The wave amplitudes that develop at any particular location depend on the background fluctuation level that is being amplified. The background level may be a result of thermal fluctuations or embryonic wave populations. The instability is assumed to be limited by convection of the waves out of the growth region, or by nonlinear saturation. The source of the wave amplification is the pitch angle anisotropy in the ring current ion distribution. In addition, wave growth rates depend sensitively on the composition of the thermal and energetic plasma [*Kozyra et al.*, 1984] and on gradients in the thermal plasma which affect the wave normal angle and wave propagation paths [*Thorne and Horne*, 1997]. Wave growth maximizes for field-aligned propagation near the equator. The wave normal angle tends to increase as waves propagate in the heterogeneous magnetospheric environment. Consequently, waves are amplified over limited spatial regions that vary in location and spatial extent as the ring current evolves during the magnetic storm interval. Wave-induced diffusion will drive the ring current ions toward marginal stability [e.g., *Gary et al.*, 1995], limiting the time interval during which the waves exist. Injections of fresh particles from the near-Earth plasma sheet into the inner magnetosphere is required to provide additional free energy to sustain wave instability.

An initial attempt to include the effects of wave-particle diffusion [*Jordanova et al.*, 1996b] into a global simulation of ring current dynamics during a modest magnetic storm was described by *Jordanova et al.* [1997]. The distribution function of energetic protons, obtained from the Michigan RAM code (which includes the effects of particle drifts, charge exchange and Coulomb scattering), was shown to be unstable to the generation of EMIC waves. Peak convective wave growth was confined to the dusk sector near the plasmapause. Proton precipitation due to adopted wave amplitudes over the zone of significant wave growth was found to be considerable locally, but it amounted to a loss of only 1–2% of the total ring current energy over the course of this modest-sized simulated storm.

An improved model of wave growth and its effects on ion diffusion and precipitation has recently been undertaken [*Kozyra et al.*, 1997] by combining the global simulation of ion dynamics during the November 1993 magnetic storm (using the Michigan RAM code) with detailed calculations of path integrated wave gain from the HOTRAY code [*Horne*, 1989; *Thorne and Horne*, 1997]. A broad zone of intense wave gain developed in the dusk sector during the main phase of the storm (Figure 19). Peak wave growth (≥100 dB) occurred in the vicinity of the plasmapause due to a combination of the available source of anisotropic ring current H^+ ions and wave guiding along the steep density gradient. An example of path integrated amplification near the plasmapause is shown in Figure 20. The wave shown was initiated at a location below the equator and propagated up to the reflection point where the frequency dropped below the bi-ion frequency ω_{bi}. This ray followed a trajectory along the edge of the steep density gradient associated with the plasmapause. As a consequence, the wave was strongly guided by the density gradient, and the wave normal angle was confined within a small cone ($|\psi| \leq 10°$) centered on the magnetic field direction over an extended region of the ray path $|\lambda| < 12°$ near the equator. Guiding by the density gradient has a pronounced effect on the net wave amplification resulting in a peak path-integrated gain $G_{peak} \approx 130$ dB. This is

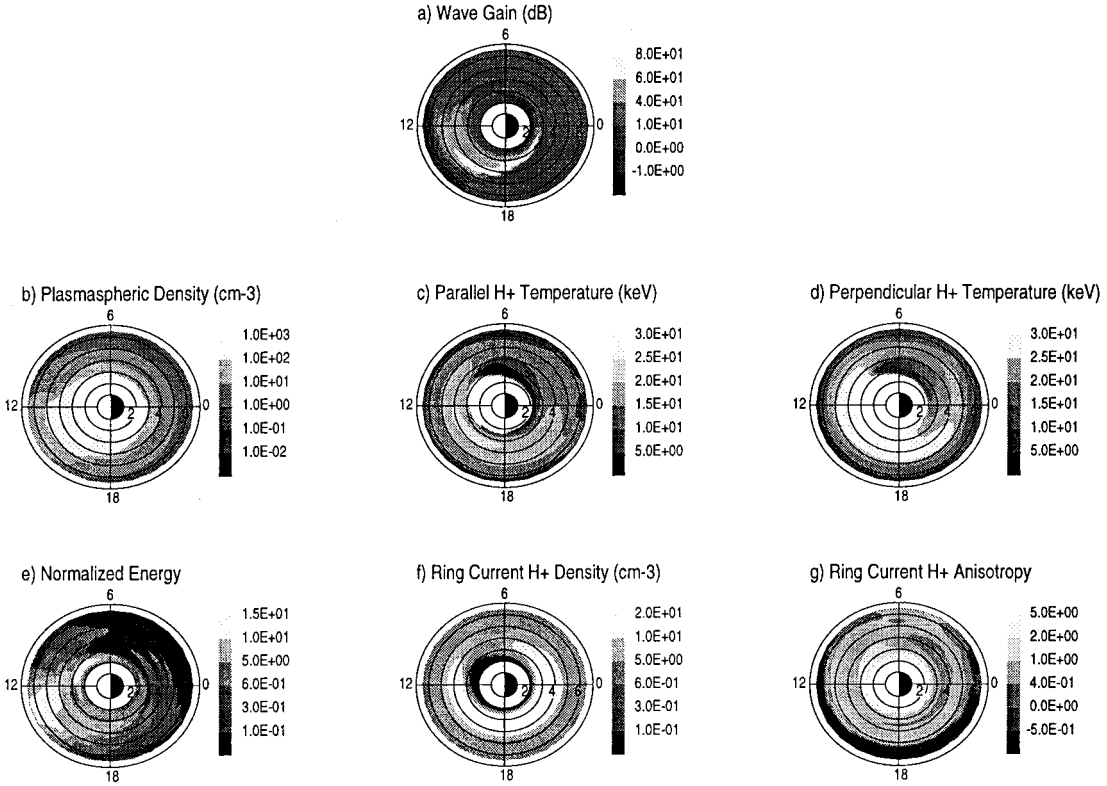

Figure 19. (a) RAM code simulation [*Kozyra et al.*, 1997] of EMIC wave gain at 0400 UT on November 4, 1993, along with associated values of (b) thermal plasmaspheric density and ring current (c) parallel and (d) perpendicular H^+ temperature, (e) parallel energy normalized to $B^2/2\mu_0$, (f) density, and (g) anisotropy.

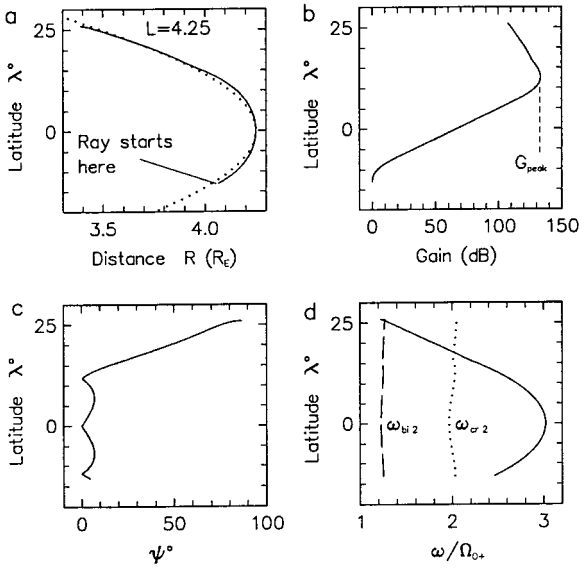

Figure 20. HOTRAY calculations [*Thorne and Horne*, 1997] of the (a) ray path, (b) path-integrated gain, (c) wave normal angle ψ, and (d) wave frequency normalized to the O^+ gyrofrequency ω/Ω_{O^+}, for guided EMIC waves launched from below the magnetic equator near $L = 4.25$.

more than sufficient to allow waves to grow from the background noise, but nonlinear processes should come into play to limit the wave amplitude under such conditions. Strong wave amplification can occur over a wide frequency band ($2.5\Omega_{O^+} \leq \omega \leq 3.4\Omega_{O^+}$) at this location.

The HOTRAY code was employed by *Thorne and Horne* [1997] to evaluate the peak path-integrated gain of the unstable band of waves at each equatorial L shell along the 1700 MLT meridian. This was used to determine the strongest amplification $G_{\max}$ over the unstable band; the results are plotted as the solid line in Figure 21. The circles on that plot are an estimate of the path-integrated gain

$$G^* = k_I \Delta s \tag{11}$$

based on the equatorial convective growth rate k_I for field-aligned waves assuming an unstable path length for amplification Δs corresponding to a $\pm 5°$ magnetic latitude path near the equator. Note that (11) provides a reasonable approximation to the exact path-integrated computations with HOTRAY throughout the plasmasphere, but it tends to underestimate the wave gain near the plasmapause where guiding of the waves becomes

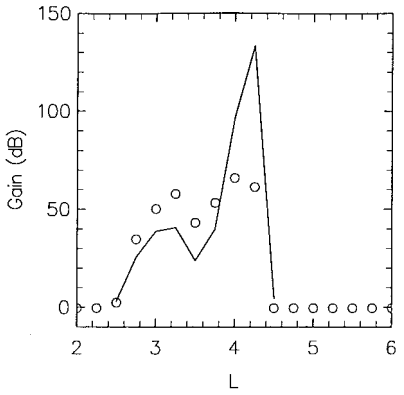

Figure 21. Maximum path-integrated gain obtained by HOTRAY (solid line) compared with equation (11) (circles) as a function of L shell. The strong enhancement in gain at L = 4.25 is due to guiding by the plasmapause density gradient [*Thorne and Horne*, 1997].

important. Although observable waves ($G \geq 30$ dB) could be excited over a broad radial range ($3.0 \leq L \leq 4.5$), the strongest waves should be confined to the region near the plasmapause.

Wave gain cannot be converted directly into wave power because information on the background embryonic noise level is unavailable. Observations indicate that a wideband amplitude of EMIC waves during storms can attain values of 1–10 nT in the vicinity of the plasmapause [*Anderson et al*., 1992b]. *Kozyra et al*. [1997] have used this constraint together with the global calculations of path-integrated gain to construct the global distribution of wave power during the November 1993 storm. This was subsequently used to evaluate the rate of ion scattering and loss to the atmosphere. The wave-induced scattering produced a strong enhancement in the proton precipitation in association with the region of EMIC wave activity (Figure 22). The integrated energy loss from the ring current due to the scattering of protons into the loss cone during interaction with the prescribed ion cyclotron waves was found to be important to the global energy balance of the ring current. With the adopted wave parameters, the wave losses caused an additional ~10-nT recovery of *Dst* (accounting for ~10% of the total ring current energy) for the one-hour period in which the effects of waves were added to the simulation of the November 1993 magnetic storm.

An important feature of the path-integrated gain shown in Figure 20 is the wave attenuation at latitudes above $\lambda \approx 12°$. This attenuation is due primarily to cyclotron resonant absorption by energetic ring current O^+. Near the equator the energy of H^+ ions resonating with the EMIC waves falls near the peak of the ring current flux distribution; this results in strong amplification of the waves by the anisotropic ring current. At

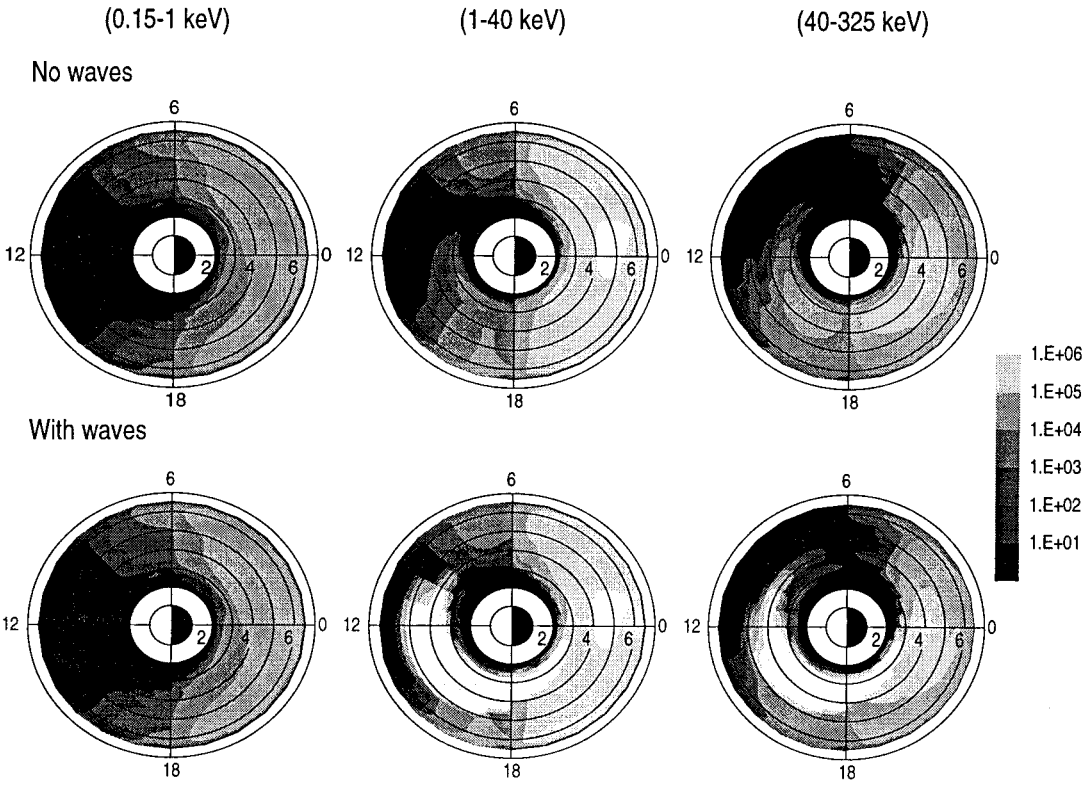

Figure 22. RAM code simulation [*Kozyra et al*., 1997] of the global pattern of total precipitating ion flux at 0500 UT on November 4, 1993, with and without wave scattering. Equatorial ion fluxes in the loss cone are averaged over pitch angle and integrated over selected energy ranges (0.15–1 keV, 1–40 keV, and 40–325 keV). The color version of this figure appears on the front cover of this issue.

higher magnetic latitudes the energy of resonating H^+ ions increases. This leads to a reduction in the number of resonating H^+ ions because the energy required for resonance now falls above the ring current flux peak, and a corresponding reduction in wave growth occurs. In contrast, for latitudes above 12° the energy of O^+ ions in resonance with the EMIC waves (generated by the ring current H^+ ions near the equator) remains close to the energy of peak O^+ fluxes in the ring current. These O^+ ions act to absorb wave energy rather than amplify the waves. This ensures that the wave is subject to net damping at high latitudes. The overall balance between cyclotron growth from ring current H^+ and damping by energetic O^+ is controlled by the relative number densities and the energy distributions of the two energetic ion populations.

For more intense geomagnetic storms the fractional composition η_{O^+} of energetic O^+ should be larger than the values (26%) specified in the RAM code simulation of the November 1993 storm. To investigate the effect of variable oxygen concentration, *Thorne and Horne* [1997] have allowed the values of η_{O^+} to increase while keeping the total number density of the ring current and the ion temperatures fixed at the nominal values obtained from the RAM code. As η_{O^+} was increased from the nominal value of 26%, they obtained a gradual decrease in the net rate of wave amplification and a stronger net attenuation at high latitudes, where the H^+ cyclotron resonant growth rate becomes ineffective. For a value of $\eta_{O^+} = 60\%$, comparable to that reported by *Daglis* [1997a] for the main phase of major magnetic storms, the peak path-integrated gain dropped below 30 dB. This would effectively suppress the excitation of EMIC waves in the band above Ω_{O^+} during such great storms. In the absence of the additional scattering loss caused by enhanced EMIC waves, the effective lifetimes for energetic H^+ ions will increase, especially at energies above 100 keV. This should allow the energy density of trapped H^+ ions to build up to much larger values for storms with a large O^+ component. It raises the interesting, but as yet unresolved, question of whether the intensity of the *Dst* depression for major storms might be modulated by the concentration of O^+ through the process of resonant interaction with EMIC waves.

The cyclotron resonant absorption of EMIC waves by energetic O^+ ions could also have important ramifications on the injection of ionospheric ions into the magnetosphere during disturbed conditions. In addition to the first-order cyclotron resonant absorption by ring current O^+, oblique EMIC wave absorption can occur during resonant interaction with lower-energy O^+ ions at frequencies near the bi-ion and second harmonic of the O^+ gyrofrequency [*Thorne and Horne*, 1993, 1994]. The absorption leads to O^+ heating perpendicular to the magnetic field. Upflowing ionospheric O^+ ions, which originate during disturbed conditions from an ion conic heating region [*Klumpar et al*., 1984; *André et al*., 1998] and are subsequently injected into the magnetosphere with a field-aligned distribution [*Daglis et al*., 1993], should be scattered into a more isotropic distribution by resonant interaction with EMIC waves. This would ensure that such ions become trapped in the magnetosphere. During storm conditions, the trapped O^+ population could exhibit further stochastic acceleration up to ring current energies by resonant interaction with intense EMIC waves [*Thorne and Horne*, 1994].

7. SUMMARY

The terrestrial ring current, an electric current flowing in a toroidal pattern in near-Earth space, has attracted major interest since the early days of space research because it causes worldwide magnetic disturbances, termed collectively as the geomagnetic storm. The development of an intense ring current is an essential part of the geomagnetic storm, while other magnetospheric current systems (such as the cross-tail current or the magnetopause current) also contribute to the storm time global magnetic disturbances [e.g., *Alexeev et al*., 1996; *Campbell*, 1996].

The immediate particle sources of the ring current are the plasma sheet and the ionosphere. Since the plasma sheet population is supplied by the ionosphere and the solar wind, the two main sources of the ring current are the terrestrial ionosphere and the solar wind. The relative contribution of the two sources is not completely clarified, but generally the contribution of the ionosphere to the ring current, mainly in the form of O^+ ions, increases with the magnitude of the storm.

The role of substorms in building up the ring current is still under dispute. According to recent studies, the storm time ring current is not created through substorm injections as its basic elements. However, substorms have an important role in releasing the high pressure built up at the boundary between the magnetotail proper and the inner magnetosphere, similar to an earthquake, and unclogging the earthward flow and injection of particles into the ring current. Furthermore, the recurrence of substorms in a storm leads to recirculation of particles between the tail and the inner magnetosphere, as well as to increased ionospheric outflow, and thereby to higher particle energies and stronger ring current.

Wave-particle interactions allow the efficient transfer of energy between different ion components of the ring current. This could contribute to the geomagnetic trapping and acceleration of ionospheric O^+ ions that are injected during the main phase of a storm. Resonant pitch angle scattering also has the potential to remove resonant ions on timescales of less than an hour; this is much shorter than the loss rate associated with collisional processes. However, since the region of intense wave scattering is expected to be localized, the global effect on ring current decay is expected to be small in comparison with charge exchange.

A most powerful tool in the efforts for comprehensive

understanding of the ring current is energetic neutral atom imaging. The potential of ENA imaging has been increasingly recognized during the last few years [*Williams*, 1990; *Akasofu*, 1991; *Williams et al*., 1992]. Since ENA spectra are strongly related to the ring current ion distributions, ENA imaging provides global information on the ring current ion population, at timescales that cannot be matched by any other method. A dedicated global imaging mission, Imager for Magnetopause-to-Aurora Global Exploration (IMAGE), which includes ENA imaging instrumentation, is scheduled for launch in the year 2000 (see *Green et al*. [1996] and http://image.gsfc.nasa.gov/). The benefits of global imaging for the construction of a coherent and comprehensive picture of the ring current spatial and temporal evolution have already been indicated by sporadic ENA measurements from the Geotail and POLAR missions.

Finally, one should note that although it is generally believed that the energy density of the ring current is dominated by ions, the precise contribution from electrons to the storm time *Dst* depression is not well known. In addition, the global structure of the convection electric field, which is primarily responsible for the energization of the ring current during a storm, is also not well established. Current modeling efforts on the development and decay of the ring current and its effect on *Dst* are seriously affected by these deficiencies. A resolution of these gaps in our understanding will be major objectives in the recently initiated Geospace Environmental Modeling (GEM) campaign to study geomagnetic storms.

GLOSSARY

Adiabatic invariants: Geomagnetically trapped charged particles execute three basic motions according to three adiabatic invariants. The first adiabatic invariant or magnetic moment μ of the particle is equal to

$$\mu = m v_\perp^2 / 2B.$$

Here μ is a constant of the cyclotron motion (gyration) of the particle in spatially and temporally varying magnetic fields **B**, as long as the rate of change of **B** is smaller than the gyrofrequency ω_c of the particle, and as long as their gyroradius is comparable to or larger than the magnetic field line curvature radius. The second adiabatic invariant is equal to

$$J = \oint p_\parallel \, dl = 2 \int_{m_1}^{m_2} m v_\parallel \, dl,$$

where $p_\parallel$ is the component of the particle momentum along the magnetic field and the integral is along the field line. J is associated with the bounce motion of the particle along field lines and between mirror points m_1 and m_2; it is invariant as long as the electromagnetic field variations have frequencies ω much smaller than the bounce frequency ω_b. As the particle bounces, it also drifts around the Earth, moving on a closed three-dimensional drift shell around the magnetic field axis. The third adiabatic invariant is the conserved magnetic flux encircled by the particles' periodic drift shell orbits:

$$\Phi = \oint v_d r \, d\psi,$$

where v_d is the sum of all perpendicular drift velocities, ψ is the azimuthal angle, and the integration is taken over a complete drift path of the particle. Φ is invariant when the frequency ω of electromagnetic field variations is much smaller than the drift frequency ω_d.

Auroral electrojet (AE) indices: The AE indices (AU, AL, and AE) provide a measure of the ground magnetic effect of the eastward and westward *auroral electrojet* currents. To calculate the AE indices, the H component of the geomagnetic field from observatories located in auroral or subauroral latitudes and relatively uniform in longitude is used. The AU and AL indices are defined by the upper and lower envelopes of the superposed perturbation ΔH from all stations. The difference between the upper and lower envelopes defines the AE index. AU and AL represent the intensity level of the eastward and westward electrojet, respectively, while AE represents the activity level of the auroral zone irrespective of local time and is often used as an indicator of substorms.

Auroral electrojets: High-latitude current flow concentrated inside the auroral oval and carrying a total current of $\sim 10^6$ A.

Betatron acceleration: Gain of energy in the direction transverse to the magnetic field, which results from the transport of charged particles into stronger magnetic fields without violation of the first adiabatic invariant.

Bi-ion frequency ω_{bi}: Electromagnetic wave resonance condition ($|k| \rightarrow \infty$) just above the heavy ion gyrofrequency, which only occurs in a multi-ion plasma.

Charge exchange: Process in which an energetic ion acquires an electron from a thermal neutral atom. As a result, the singly charged energetic ion is neutralized, thus becoming an energetic neutral atom (ENA); conversely, the thermal atom becomes a thermal ion.

Cleft: A funnel-like region of weak magnetic field in the dayside high-latitude magnetosphere (Figure 1), where both precipitation of electrons to the ionosphere and outflow of ionospheric ions to the magnetosphere occurs.

Coulomb collisions: Collisional interactions between charged particles due to their electric fields.

Current sheet or cross-tail current: A current that flows across the midplane of the magnetotail and connects with the magnetopause currents at the flanks of the tail (Figure 1).

Dipolarization: During the substorm growth phase, the nightside magnetic field obtains a stretched config-

uration due to the enhancement and earthward displacement of the near-Earth cross-tail current sheet. At substorm onset the magnetic field relaxes from the stretched configuration to a more dipole-like configuration, because of a disruption or diversion or reduction of the current sheet. This field relaxation is called dipolarization.

***Dst* index:** Index constructed from magnetograms of several low-latitude stations, and provides information on the intensity of magnetic storms. Because *Dst* involves deviations in the horizontal H component of the geomagnetic field from quiet-time values and the effect of magnetic storms is a global reduction of H, *Dst* is negative during storms. A larger negative *Dst* means a more intense storm, and generally a more intense ring current. Two examples of the storm time *Dst* variation are shown in the bottom panels of Figures 4 and 5. However, *Dst* is not a perfect measure of the ring current intensity because it is influenced by other magnetospheric currents (such as the cross-tail current) as well.

Electromagnetic ion cyclotron (EMIC) waves: Electromagnetic waves caused by ion gyration at frequency bands below the proton gyrofrequency, which interact strongly with ring current ions. The waves are basically left-hand polarized for field-aligned propagation.

Energetic neutral atoms (ENA): Atoms with energies of a few keV to hundreds of keV emitted from hot plasmas when energetic ions undergo charge-exchange interactions. In the case of the Earth magnetosphere, ENA are produced primarily through charge exchange between singly charged energetic ions and the cold neutral hydrogen of the geocorona. The neutrals produced by charge exchange leave the interaction region with essentially the same energy and direction as the incident ion.

Fermi acceleration: Gain of energy in the direction parallel to the magnetic field, which results from field line contraction (i.e. from a shortening of the bounce path of the particle) without violation of the second adiabatic invariant.

First adiabatic invariant: See "adiabatic invariants."

Geocorona: An exospheric extension of relatively cold (~1000 K) neutral atoms (mainly hydrogen), which resonantly scatter solar Lyman α radiation.

Gyration or cyclotron motion: The motion of a charged particle under the action of the Lorentz force due to a magnetic field. The trajectory is circular when the velocity of the particle parallel to the magnetic field is zero, or a helix when the parallel velocity is nonzero (Figure 2). The radius of the circular or helicoidal cyclotron motion is called the gyroradius and is equal to $r_c = m v_\perp / qB$, while the frequency of gyration is called gyrofrequency or cyclotron frequency and is equal to $\omega_c = qB/m$, where q is the charge and m is the mass of the particle.

Interplanetary magnetic field (IMF): Magnetic field resulting from the outward transport of the solar magnetic field by the expanding solar plasma known as the solar wind.

Ion conic: Transversely heated ions that originate in the ionosphere and have an angular distribution function that is peaked at some angle to the magnetic field direction.

Ionosphere: Solar ultraviolet light impinging on the Earth's atmosphere ionizes a fraction of the neutral atmosphere. At altitudes above ~80 km, collisions are too infrequent to result in rapid recombination and a partially ionized magnetized plasma called the ionosphere is formed. The ionosphere is a relatively thin layer, extending to an altitude of ~500 km. Typical electron densities and temperatures in the midlatitude ionosphere are $n_e \approx 10^5$ cm^{-3} and $T_e \approx 10^3$ K. The magnetic field strength is of the order of 10^4 nT.

keV: Kiloelectron volt, a unit of energy: x keV correspond to the energy gained by a singly charged particle that is accelerated across a potential difference of x kV.

***L* parameter:** The equation of a geomagnetic field line is $r = L \cos^2 \lambda$, where r is geocentric distance from the center of Earth, λ is the magnetic latitude. The L parameter is the distance in Earth radii (R_E) from the center of Earth to the point where a geomagnetic field line crosses the equator ($\lambda = 0$). L is useful in identifying field lines and magnetic drift shells.

Left-hand or right-hand polarization: Sense of rotation of the electric vector for field-aligned electromagnetic waves.

Linear polarization: The wave electric vector is confined to oscillate along a specified line.

Loss cone: Pitch angle range for particle mirror points below the top of the atmosphere. Particles with such pitch angles are removed by collisions with the atmosphere.

Lower hybrid frequency ω_{LHR}: Wave resonance condition ($|k| \to \infty$) between the ion and electron gyrofrequencies.

Magnetosonic waves: Low-frequency (near the ion gyrofrequency) electromagnetic waves, which are right-hand polarized for field-aligned propagation.

Magnetosphere: A large "cavity" in space resulting from the interaction of a planetary magnetic field and the solar wind (Figure 1). It is defined as the region of space in which the planetary magnetic field has a dominant control over the motion of charged particles. The terrestrial magnetosphere extends up to ~10 R_E in the sunward direction and to several hundred R_E in the antisunward direction. Within the magnetosphere there are diverse populations of hot collisionless plasmas. The boundary layer between the magnetosphere and the solar wind is the magnetopause, while the comet-like part of the magnetosphere, which stretches antisunward far beyond lunar orbit, is the magnetotail.

Mirror latitude: As a geomagnetically trapped particle moves along a magnetic field line from the equator towards higher latitude it encounters increasing B; to conserve its magnetic moment (the first adiabatic invariant) its pitch angle increases. Eventually it becomes 90° and the particle is reflected back along the field line (Figure 2). The latitude of the deflection point is called mirror latitude and is dependent on the equatorial velocity pitch angle of the particle and the magnetic field geometry.

Pitch angle: Angle between the velocity vector of a charged particle and the ambient magnetic field vector (Figure 2).

Plasma beta (β): The average ratio of particle pressure to magnetic field pressure $p/(B^2/2\mu_0)$, which is a measure of their relative importance.

Plasmapause: Outer boundary of the plasmasphere at a highly variable altitude between ~2.5 and 6 R_E, marked by a steep drop of the plasma density. See "plasmasphere."

Plasma sheet: Region in the midplane of the magnetotail, with a radius of ~5 R_E, containing most of the magnetotail plasma. Near the Earth it reaches down to the high-latitude auroral ionosphere along the field lines. Average electron densities and temperatures in the plasma sheet are $n_e \approx 0.5$ cm^{-3} and $T_e \approx 5 \times 10^6$ K, with $B \approx 10$ nT.

Plasmasphere: A torus-shaped volume in the innermost magnetosphere. It contains a cool but dense plasma of ionospheric origin ($n_e \geq 5 \times 10^2$ cm^{-3}, $T_e \approx 5 \times 10^3$ K), which corotates with the Earth. In the equatorial plane the plasmasphere extends out to about 4 R_E, where the density drops down sharply to about 1 cm^{-3}. This boundary is called the plasmapause.

***R_E*:** The average Earth radius, a common unit in magnetospheric physics, equivalent to 6371 km.

Second adiabatic invariant: See "adiabatic invariants."

Solar wind: A plasma of protons and electrons, with an admixture of He^{++} and other lesser solar ions, streaming continuously together with the solar magnetic field from the solar atmosphere out to the solar system with speeds of ~200–1000 km s^{-1}.

Substorm: Basic disturbance in the terrestrial magnetosphere, involving successive reconfigurations of the geomagnetic field and explosive dissipation of energy at the high-latitude ionosphere (auroral displays), the inner plasma sheet (acceleration of energetic ions) and the distant magnetotail (formation of magnetic neutral lines and plasmoids). The energy is provided by the solar wind and is temporarily stored in the form of increased magnetic flux in the magnetotail.

Thermosphere: High-temperature ($T > 1000$ K) region of the upper atmosphere above ~100 km.

Wave normal angle: Angle ψ between the wave propagation vector **k** and the ambient magnetic field **B**.

Whistler mode waves: Right-hand-polarized electromagnetic waves caused by electron gyration at frequencies below the electron gyrofrequency.

ACKNOWLEDGMENTS. We would like to thank the referees for their constructive comments. Furthermore, we would like to thank L. F. Bargatze, M. Hesse, Y. Kamide, A. Milillo, and V. O. Papitashvili for helpful discussions and suggestions. Special thanks are due to P. W. Daly for his invaluable help with L^AT_EX. Parts of this review were written while the lead author (I.A.D.) was a visiting faculty member at the Solar-Terrestrial Environment Laboratory, Nagoya University. This work was supported in part by NASA grant NAG54680, NSF grant AMT 97 29021, and PENED grant 878/1995 of the Greek General Secretariat of Research and Technology.

James Horwitz was the Editor responsible for this paper. He thanks Janet Kozyra, Doug Hamilton, and Mei-Ching Fok for technical reviews, and Craig Bina for the cross-disciplinary review.

REFERENCES

Abe, T., B. A. Whalen, A. W. Yau, R. E. Horita, S. Watanabe, and E. Sagawa, Exos D (Akebono) suprathermal mass spectrometer observations of the polar wind, *J. Geophys. Res.*, *98*, 11,191–11,203, 1993.

Aggson, T. L., and J. P. Heppner, Observations of large transient magnetospheric electric fields, *J. Geophys. Res.*, *82*, 5155–5164, 1977.

Aggson, T. L., J. P. Heppner, and N. C. Maynard, Observations of large magnetospheric electric fields during the onset phase of a substorm, *J. Geophys. Res.*, *88*, 3981–3990, 1983.

Akasofu, S.-I., *Polar and Magnetospheric Substorms*, D. Reidel, Norwell, Mass., 1968.

Akasofu, S.-I., Auroral phenomena, in *Auroral Physics*, edited by C.-L. Meng, M. J. Rycroft, and L. A. Frank, pp. 3–12, Cambridge Univ. Press, New York, 1991.

Akasofu, S.-I., S. Chapman, and D. Venkatesan, The main phase of great magnetic storms, *J. Geophys. Res.*, *68*, 3345–3350, 1963.

Alexeev, I. I., E. S. Belenkaya, V. V. Kalegaev, Y. I. Feldstein, and A. Grafe, Magnetic storms and magnetotail currents, *J. Geophys. Res.*, *101*, 7737–7747, 1996.

Anderson, B. J., and S. A. Fuselier, Response of thermal ions to electromagnetic ion cyclotron waves, *J. Geophys. Res.*, *99*, 19,413–19,425, 1994.

Anderson, B. J., and D. C. Hamilton, Electromagnetic ion cyclotron waves simulated by modest magnetospheric compressions, *J. Geophys. Res.*, *98*, 11,369–11,382, 1993.

Anderson, B. J., K. Takahashi, R. E. Erlandson, and L. J. Zanetti, Pc1 pulsations observed by AMPTE/CCE in the Earth's outer atmosphere, *Geophys. Res. Lett.*, *17*, 1853–1856, 1990.

Anderson, B. J., R. E. Erlandson, and L. J. Zanetti, A statistical study of Pc1–2 magnetic pulsations in the equatorial magnetosphere, 1, Equatorial occurrence distributions, *J. Geophys. Res.*, *97*, 3075–3088, 1992a.

Anderson, B. J., R. E. Erlandson, and L. J. Zanetti, A statistical study of Pc1–2 magnetic pulsations in the equatorial magnetosphere, 2, Wave properties, *J. Geophys. Res.*, *97*, 3089–3101, 1992b.

Anderson, B. J., R. E. Denton, G. Ho, D. C. Hamilton, S. A. Fuselier, and R. J. Strangeway, Observational test of local proton cyclotron instability in the Earth's magnetosphere, *J. Geophys. Res.*, *101*, 21,527–21,543, 1996.

André, M., P. Norquist, L. Anderson, L. Eliasson, A. I. Eriksson, L. Blomberg, R. E. Erlandson, and J. Waldemark, Ion energization mechanisms at 1700 km in the auroral region, *J. Geophys. Res*., *103*, 4199–4222, 1998.

Ashour-Abdalla, M., J. P. Berchem, J. Büchner, and L. M. Zelenyi, Shaping of the magnetotail from the mantle: Global and local structuring, *J. Geophys. Res*., *98*, 5651–5676, 1993.

Axford, W. I., On the origin of radiation belt and auroral primary ions, in *Particles and Fields in the Magnetosphere*, edited by B. M. McCormac, pp. 46–59, D. Reidel, Norwell, Mass., 1970.

Baker, D. N., Particle and field signatures of substorms in the near magnetotail, in *Magnetic Reconnection in Space and Laboratory Plasmas*, *Geophys. Monogr. Ser*., vol. 30, edited by E. W. Hones Jr., vol. 30, pp. 193–202, AGU, Washington, D. C., 1984.

Baker, D. N., and R. L. McPherron, Extreme energetic particle decreases near geostationary orbit: A manifestation of current diversion within the inner plasma sheet, *J. Geophys. Res*., *95*, 6591–6599, 1990.

Baker, D. N., T. A. Fritz, W. Lennartsson, B. Wilken, H. W. Kroehl, and J. Birn, The role of heavy ions in the localization of substorm disturbances on March 22, 1979: CDAW 6, *J. Geophys. Res*., *90*, 1273–1281, 1985.

Baker, D. N., R. A. Goldberg, F. A. Herrero, J. B. Blake, and L. B. Callis, Satellite and rocket studies of relativistic electrons and their influence on the middle atmosphere, *J. Atmos. Terr. Phys*., *55*, 1619–1628, 1993.

Balsiger, H., P. Eberhardt, J. Geiss, and D. T. Young, Magnetic storm injection of 0.9- to 16-keV/*e* solar and terrestrial ions into the high-altitude magnetosphere, *J. Geophys. Res*., *85*, 1645–1662, 1980.

Banks, P. M., and T. E. Holzer, High-latitude plasma transport: The polar wind, *J. Geophys. Res*., *74*, 6317–6332, 1969.

Barabash, S., P. C. Brandt, O. Norberg, R. Lundin, E. C. Roelof, C. J. Chase, B. H. Mauk, and H. Koskinen, Energetic neutral atom imaging by the ASTRID microsatellite, *Adv. Space Res*., *20*(4/5), 1055–1060, 1997.

Baumjohann, W., The near-Earth plasma sheet: An AMPTE/IRM perspective, *Space Sci. Rev*., *64*, 141–163, 1993.

Baumjohann, W., and R. A. Treumann, *Basic Space Plasma Physics*, Imperial Coll. Press, London, 1996.

Baumjohann, W., Y. Kamide, and R. Nakamura, Substorms, storms, and the near-Earth tail, *J. Geomagn. Geoelectr*., *48*, 177–185, 1996.

Boardsen, S. A., D. L. Gallagher, D. A. Gurnett, W. K. Peterson, and J. L. Green, Funnel-shaped, low-frequency equatorial waves, *J. Geophys. Res*., *97*, 14,967–14,976, 1992.

Brandt, P. C., S. Barabash, O. Norberg, R. Lundin, E. C. Roelof, C. J. Chase, B. H. Mauk, and M. Thomsen, ENA imaging from the Swedish microsatellite ASTRID during the magnetic storm of 8 February 1995, *Adv. Space Res*., *20*(4/5), 1061–1066, 1997.

Breus, T. K., G. Cornélissen, F. Halberg, and A. E. Levitin, Temporal associations of life with solar and geophysical activity, *Ann. Geophys*., *13*, 1211–1222, 1995.

Büchner, J., and L. M. Zelenyi, Regular and chaotic charged particle motion in magnetotaillike field reversals, 1, Basic theory of trapped motion, *J. Geophys. Res*., *94*, 11,821–11,842, 1989.

Burns, A. G., T. L. Killeen, W. Deng, G. R. Carignan, and R. G. Roble, Geomagnetic storm effects in the low- to middle-latitude upper thermosphere, *J. Geophys. Res*., *100*, 14,673–14,691, 1995.

Campbell, W. H., Geomagnetic storms, the Dst ring-current myth and lognormal distributions, *J. Atmos. Terr. Phys*., *58*, 1171–1187, 1996.

Carovillano, R. L., and G. L. Siscoe, Energy and momentum theorems in magnetospheric processes, *Rev. Geophys*., *11*, 289–353, 1973.

Chamberlain, J. W., Planetary coronae and atmospheric evaporation, *Planet. Space Sci*., *11*, 901–960, 1963.

Chandler, M. O., J. H. Waite Jr., and T. E. Moore, Observations of polar ion outflows, *J. Geophys. Res*., *96*, 1421–1428, 1991.

Chapman, S., An outline of a theory of magnetic storms, *Proc. Roy. Soc. London*, *Ser. A*, *95*, 61, 1919.

Chapman, S., Earth storms: Retrospect and prospect, *J. Phys. Soc. Jpn*., *17*, suppl. A-I, 6–16, 1962.

Chapman, S., and V. C. A. Ferraro, A new theory of magnetic storms, *Nature*, *126*, 129–130, 1930.

Chapman, S., and V. C. A. Ferraro, A new theory of magnetic storms, *J. Geophys. Res*., *36*, 77–97, 1931.

Chappell, C. R., T. E. Moore, and J. H. Waite Jr., The ionosphere as a fully adequate source of plasma for the Earth's magnetosphere, *J. Geophys. Res*., *92*, 5896–5910, 1987.

Chen, J., and P. J. Palmadesso, Chaos and nonlinear dynamics of single-particle orbits in a magnetotail-like magnetic field, *J. Geophys. Res*., *91*, 1499–1508, 1986.

Chen, M. W., L. Lyons, and M. Shultz, Simulations of phase space distributions of storm time proton ring current, *J. Geophys. Res*., *99*, 5745–5759, 1994.

Christon, S. P., D. C. Hamilton, G. Gloeckler, T. E. Eastman, and F. M. Ipavich, High charge state carbon and oxygen ions in Earth's equatorial quasi-trapping region, *J. Geophys. Res*., *99*, 13,465–13,488, 1994.

Christon, S. P., G. Gloeckler, D. J. Williams, R. W. McEntire, and A. T. Y. Lui, The downtail distance variation of energetic ions in Earth's magnetotail region: Geotail measurements at $X > -208R_E$, *J. Geomagn. Geoelectr*., *48*, 615–627, 1996.

Cladis, J. B., and W. E. Francis, The polar ionosphere as a source of the storm time ring current, *J. Geophys. Res*., *90*, 3465–3473, 1985.

Cladis, J. B., and W. E. Francis, Distribution in magnetotail of O^+ ions from cusp/cleft ionosphere: A possible substorm trigger, *J. Geophys. Res*., *97*, 123–130, 1992.

Cornwall, J. M., On the role of charge exchange in generating unstable waves in the ring current, *J. Geophys. Res*., *82*, 1188–1196, 1977.

Cornwall, J. M., F. V. Coroniti, and R. M. Thorne, Turbulent loss of ring current protons, *J. Geophys. Res*., *75*, 4699–4709, 1970.

Cowley, S. W. H., Pitch angle dependence of the charge-exchange lifetime of ring current ions, *Planet. Space Sci*., *25*, 385–393, 1977.

Daglis, I. A., The role of magnetosphere-ionosphere coupling in magnetic storm dynamics, in *Magnetic Storms*, *Geophys. Monogr. Ser*., vol. 98, edited by B. T. Tsurutani et al., pp. 107–116, AGU, Washington, D. C., 1997a.

Daglis, I. A., Terrestrial agents in the realm of space storms: Missions study oxygen ions, *Eos Trans. AGU*, *24*, 245–251, 1997b.

Daglis, I. A., and W. I. Axford, Fast ionospheric response to enhanced activity in geospace: Ion feeding of the inner magnetotail, *J. Geophys. Res*., *101*, 5047–5065, 1996.

Daglis, I. A., and S. Livi, Merits for substorm research from imaging of charge-exchange neutral atoms, *Ann. Geophys*., *13*, 505–516, 1995.

Daglis, I. A., N. P. Paschalidis, E. T. Sarris, W. I. Axford, G. Kremser, B. Wilken, and G. Gloeckler, Statistical features of the substorm expansion-phase as observed by AMPTE/CCE, in *Magnetospheric Substorms*, *Geophys. Monogr. Ser*., vol. 64, edited by J. R. Kan et al., pp. 323–332, AGU, Washington, D. C., 1991a.

Daglis, I. A., E. T. Sarris, and G. Kremser, Ionospheric con-

tribution to the cross-tail current during the substorm growth phase, *J. Atmos. Terr. Phys*., *53*, 1091–1098, 1991b.

Daglis, I. A., E. T. Sarris, and B. Wilken, AMPTE/CCE CHEM observations of the ion population at geosynchronous altitudes, *Ann. Geophys*., *11*, 685–696, 1993.

Daglis, I. A., S. Livi, E. T. Sarris, and B. Wilken, Energy density of ionospheric and solar wind origin ions in the near-Earth magnetotail during substorms, *J. Geophys. Res*., *99*, 5691–5703, 1994.

Daglis, I. A., S. Livi, and B. Wilken, Benefits for the substorm research from the Cluster mission, in *Proceedings of the Cluster Workshops*, edited by C. Mattok, *ESA Spec. Publ*., *SP-371*, 259–262, 1995.

Daglis, I. A., W. I. Axford, S. Livi, B. Wilken, M. Grande, and F. Søraas, Auroral ionospheric ion feeding of the inner plasma sheet during substorms, *J. Geomagn. Geoelectr*., *48*, 729–739, 1996.

Daglis, I. A., G. Kasotakis, E. T. Sarris, Y. Kamide, S. Livi, and B. Wilken, Variations of the ion composition during an intense magnetic storm and their consequences, *Phys. Chem. Earth*, *24*, 229–232, 1999a.

Daglis, I. A., Y. Kamide, C. Mouikis, G. D. Reeves, E. T. Sarris, K. Shiokawa, and B. Wilken, "Fine structure" of the storm-substorm relationship, *Adv. Space Res*., in press, 1999b.

Delcourt, D. C., J.-A. Sauvaud, and T. E. Moore, Cleft contribution to ring current formation, *J. Geophys. Res*., *95*, 20,937–20,943, 1990a.

Delcourt, D. C., J.-A. Sauvaud, and A. Pedersen, Dynamics of single-particle orbits during substorm expansion phase, *J. Geophys. Res*., *95*, 20,853–20,865, 1990b.

Delcourt, D. C., T. E. Moore, and J.-A. Sauvaud, Gyro-phase effects near the storm-time boundary of energetic plasma, *Geophys. Res. Lett*., *18*, 1485–1488, 1991.

De Michelis, P., and S. Orsini, Energetic neutral atoms propagating toward the Earth: Analysis of the reduction rate due to ionospheric and atmospheric interactions, *J. Geophys. Res*., *102*, 185–194, 1997.

De Michelis, P., I. A. Daglis, and G. Consolini, Reconstruction of the terrestrial ring current derived from AMPTE/CCE-CHEM, *J. Geophys. Res*., *102*, 14,103–14,111, 1997.

Dessler, A. J., and W. B. Hanson, Possible energy source for the aurora, *Astrophys. J*., *134*, 1024–1025, 1961.

Dessler, A. J., and E. N. Parker, Hydromagnetic theory of geomagnetic storms, *J. Geophys. Res*., *64*, 2239–2252, 1959.

Dungey, J. W., Interplanetary magnetic field and the auroral zones, *Phys. Rev. Lett*., *6*, 47–48, 1961.

Erickson, G. M., and R. A. Wolf, Is steady convection possible in the Earth's magnetotail?, *Geophys. Res. Lett*., *7*, 897–900, 1980.

Feldstein, Y. I., A. E. Levitin, S. A. Golyshev, L. A. Dremukhina, U. B. Vestchezerova, T. E. Valchuk, and A. Grafe, Ring current and auroral electrojets in connection with interplanetary medium parameters during magnetic storm, *Ann. Geophys*., *12*, 602–611, 1994.

Fite, W. L., T. R. Brackman, and W. R. Snow, Charge transfer in proton-hydrogen atom collisions, *Phys. Rev*., *112*, 1161–1169, 1958.

Fitzgerald, G. F., Sunspots and magnetic storms, *Electrician*, *30*, 48, 1892.

Fok, M.-C., J. U. Kozyra, A. F. Nagy, and T. E. Cravens, Lifetime of ring current particles due to Coulomb collisions in the plasmasphere, *J. Geophys. Res*., *96*, 7861–7867, 1991.

Fok, M.-C., J. Kozyra, A. Nagy, C. Ramussen, and V. Khazanov, Decay of equatorial ring current ions and associated aeronomical consequences, *J. Geophys. Res*., *98*, 19,381–19,393, 1993.

Fok, M.-C., T. E. Moore, J. U. Kozyra, G. C. Ho, and D. C. Hamilton, Three-dimensional ring current decay model, *J. Geophys. Res*., *100*, 9619–9632, 1995.

Fok, M.-C., T. E. Moore, and M. E. Greenspan, Ring current development during storm main phase, *J. Geophys. Res*., *101*, 15,311–15,322, 1996.

Frank, L. A., On the extraterrestrial ring current during geomagnetic storms, *J. Geophys. Res*., *72*, 3753–3767, 1967.

Gary, S. P., M. F. Thompson, L. Yin, and D. Winske, Electromagnetic proton cyclotron instability: Interaction with magnetosphere protons, *J. Geophys. Res*., *100*, 21,961–21,972, 1995.

Gazey, N. G. J., et al., EISCAT/CRRES observations: Nightside ionospheric ion outflow and oxygen-rich substorm injections, *Ann. Geophys*., *14*, 1032–1043, 1996.

Gendrin, R., and A. Roux, Energization of helium ions by proton-induced hydromagnetic waves, *J. Geophys. Res*., *85*, 4577–4586, 1980.

Gendrin, R., M. Ashour-Abdalla, Y. Omura, and K. Quest, Linear analysis of ion cyclotron interaction in a multicomponent plasma, *J. Geophys. Res*., *89*, 9119–9124, 1984.

Ghielmetti, A. G., R. G. Johnson, R. D. Sharp, and E. G. Shelley, The latitudinal, diurnal, and altitudinal distributions of upward flowing energetic ions of ionospheric origin, *Geophys. Res. Lett*., *5*, 59–62, 1978.

Gloeckler, G., and D. C. Hamilton, AMPTE ion composition results, *Phys. Scr*., *T18*, 73–84, 1987.

Gloeckler, G., and K. C. Hsieh, Time-of-flight technique identification at energies from 2 to 400 keV/nucleon, *Nucl. Instr. and Meth*., *165*, 537–544, 1979.

Gloeckler, G., F. M. Ipavich, D. Hovestadt, M. Scholer, A. B. Galvin, and B. Klecker, Characteristics of suprathermal H^+ and He^{++} in plasmoids in the distant magnetotail, *Geophys. Res. Lett*., *11*, 1030–1033, 1984.

Gloeckler, G., B. Wilken, W. Stüdemann, F. M. Ipavich, D. Hovestadt, D. C. Hamilton, and G. Kremser, First composition measurement of the bulk of the storm-time ring current (1 to 300 keV/e) AMPTE/CCE, *Geophys. Res. Lett*., *12*, 325–328, 1985a.

Gloeckler, G., et al., The charge-energy-mass (CHEM) spectrometer for 0.3 to 300 keV/*e* ions on the AMPTE/CCE, *IEEE Trans. Geosci. Remote Sens*., *GE-23*, 234–240, 1985b.

Gomberoff, L., and R. Neira, Convective growth rate of ion cyclotron waves in a H^+-He^+ and H^+-He^+-O^+ plasma, *J. Geophys. Res*., *88*, 2170–2174, 1983.

Gonzalez, W. D., B. T. Tsurutani, A. L. C. Gonzalez, E. J. Smith, F. Tang, and S.-I. Akasofu, Solar wind-magnetosphere coupling during intense magnetic storms (1978–1979), *J. Geophys. Res*., *94*, 8835–8851, 1989.

Gonzalez, W. D., J. A. Joselyn, Y. Kamide, H. W. Kroehl, G. Rostoker, B. T. Tsurutani, and V. M. Vasyliunas, What is a geomagnetic storm?, *J. Geophys. Res*., *99*, 5771–5792, 1994.

Gorney, D. J., A. Clarke, D. Croley, J. F. Fennell, J. G. Luhmann, and P. F. Mizera, The distribution of ion beams and conics below 8000 km, *J. Geophys. Res*., *86*, 83–89, 1981.

Green, J. L., S. F. Fung, and J. L. Burch, Application of magnetospheric imaging techniques to global substorm dynamics, in *Third International Conference on Substorms* (*ICS-3*), edited by E. J. Rolfe and B. Kaldeich, *Eur. Space Agency Spec. Publ*., *ESA SP-389*, 655–661, Paris, 1996.

Gurnett, D. A., Plasma wave interactions with energetic ions near the magnetic equator, *J. Geophys. Res*., *81*, 2765–2770, 1976.

Hamilton, D. C., G. Gloeckler, F. M. Ipavich, W. Stüdemann, B. Wilken, and G. Kremser, Ring current development during the great geomagnetic storm of February 1986, *J. Geophys. Res*., *93*, 14,343–14,355, 1988.

Hedin, A. E., MSIS-86 thermospheric model, *J. Geophys. Res*., *92*, 4649–4662, 1987.

Henderson, M. G., G. D. Reeves, H. E. Spence, R. B. Sheldon, A. M. Jorgensen, J. B. Blake, and J. F. Fennell, First energetic neutral atom images from Polar, *Geophys. Res. Lett*., *24*, 1167–1170, 1997.

Hesse, M., et al., Imaging ion outflow in the high-latitude magnetosphere using low-energy neutral atoms, in *Instrumentation for Magnetospheric Imagery II*, edited by S. Chakrabarti, *Proc. SPIE Int. Soc. Opt. Eng*., *2008*, 83–92, 1993a.

Hesse, M., et al., Imaging ion outflow in the high-latitude magnetosphere using low-energy neutral atoms, *Opt. Eng*., *32*(12), 3153–3160, 1993b.

Hill, T. W., Origin of the plasma sheet, *Rev. Geophys*., *12*, 379–388, 1974.

Hirahara, M., T. Mukai, T. Terasawa, S. Machida, Y. Saito, T. Yamamoto, and S. Kokubun, Cold dense ion flows with multiple components observed in the distant tail lobe by Geotail, *J. Geophys. Res*., *101*, 7769–7784, 1996.

Ho, C. W., J. L. Horwitz, and T. E. Moore, Observations and simulations of centrifugally-accelerated polar O^+ outflows, in *Proceedings of International Conference on Substorms 2*, edited by J. R. Kan, J. D. Craven, and S.-I. Akasofu, pp. 577–581, Univ. of Alaska, Fairbanks, 1994.

Hoffman, R. A., and W. H. Dodson, Light ion concentrations and fluxes in the polar regions during magnetically quiet times, *J. Geophys. Res*., *85*, 626–632, 1980.

Horne, R. B., Path-integrated growth of electrostatic waves: The generation of terrestrial myriametric radiation, *J. Geophys. Res*., *94*, 8895–8909, 1989.

Horne, R. B., and R. M. Thorne, On the preferred source location for the convective amplification of ion-cyclotron waves, *J. Geophys. Res*., *98*, 9223–9247, 1993.

Horne, R. B., and R. M. Thorne, Convective instabilities of electromagnetic ion cyclotron waves in the outer magnetosphere, *J. Geophys. Res*., *99*, 17,259–17,273, 1994.

Horne, R. B., and R. M. Thorne, Wave heating of He^+ by electromagnetic ion-cyclotron waves in the outer magnetosphere: Heating near the H^+-He^+ bi-ion resonance frequency, *J. Geophys. Res*., *102*, 11,457–11,471, 1997.

Horwitz, J. L., The ionosphere as a source for magnetospheric ions, *Rev. Geophys*., *20*, 929–952, 1982.

Horwitz, J. L., The ionosphere's wild ride in outer space, *U.S. Natl. Rep. Int. Union Geod. Geophys. 1991–1994*, *Rev. Geophys*., *33*, 703–708, 1995.

Horwitz, J. L., and M. Lockwood, The cleft ion fountain: A two-dimensional kinetic model, *J. Geophys. Res*., *90*, 9749–9762, 1985.

Horwitz, J. L., C. J. Pollock, T. E. Moore, W. K. Peterson, J. L. Burch, J. D. Winningham, J. D. Craven, L. A. Frank, and A. Persoon, The polar cap environment of outflowing O^+, *J. Geophys. Res*., *97*, 8361–8379, 1992.

Hovestadt, D., and M. Scholer, Radiation belt-produced energetic hydrogen in interplanetary space, *J. Geophys. Res*., *81*, 5039–5042, 1976.

Hultqvist, B., Extraction of ionospheric plasma by magnetospheric processes, *J. Atmos. Terr. Phys*., *53*, 3–15, 1991.

Hultqvist, B., R. Lundin, K. Stasiewicz, L. Block, P.-A. Lundqvist, G. Gustafson, H. Kaskinen, A. Bahnsen, T. A. Potemra, and L. J. Zanetti, Simultaneous observations of upward moving field-aligned electrons and ions on auroral zone field lines, *J. Geophys. Res*., *93*, 9765–9776, 1988.

Ishida, I., S. Kokubun, and R. L. McPherron, Substorm effects on spectral structures of Pc1 waves at synchronous orbit, *J. Geophys. Res*., *92*, 143–158, 1987.

Ishimoto, M., M. R. Torr, P. G. Richards, and D. G. Torr, The role of energetic O^+ precipitation in midlatitude aurora, *J. Geophys. Res*., *91*, 5793–5802, 1986.

Iyemori, T., and D. R. K. Rao, Decay of the Dst field of geomagnetic disturbance after substorm onset and its implication to storm-substorm relation, *Ann. Geophys*., *14*, 608–618, 1996.

Jordanova, V. K., J. U. Kozyra, G. Khazanov, A. F. Nagy, C. E. Rasmussen, and M.-C. Fok, A bounce-averaged kinetic model of the ring current ion population, *Geophys. Res. Lett*., *21*, 2785–2788, 1994.

Jordanova, V. K., L. M. Kistler, J. U. Kozyra, G. V. Khazanov, and A. F. Nagy, Collisional losses of ring current ions, *J. Geophys. Res*., *101*, 111–126, 1996a.

Jordanova, V. K., J. U. Kozyra, and A. F. Nagy, Effects of heavy ions on the quasi-linear diffusion coefficients from resonant interactions with EMIC waves, *J. Geophys. Res*., *101*, 19,771–19,778, 1996b.

Jordanova, V. K., J. U. Kozyra, A. F. Nagy, and G. V. Khazanov, Kinetic model of the ring current–atmosphere interaction, *J. Geophys. Res*., *102*, 14,279–14,291, 1997.

Jorgensen, A. M., H. E. Spence, H. E. Henderson, M. G. Reeves, M. Sugiura, and T. Kamei, Global energetic neutral atom (ENA) measurements and their association with the *Dst* index, *Geophys. Res. Lett*., *24*, 3173–3176, 1997.

Kamide, Y., Relationship between substorms and storms, in *Dynamics of the Magnetosphere*, edited by S.-I. Akasofu, pp. 425–443, D. Reidel, Norwell, Mass., 1979.

Kamide, Y., Is substorm occurrence a necessary condition for a magnetic storm?, *J. Geomagn. Geoelectr*., *44*, 109–117, 1992.

Kamide, Y., N. Yokoyama, W. D. Gonzalez, B. T. Tsurutani, I. A. Daglis, A. Brekke, and S. Masuda, Two-step development of geomagnetic storms, *J. Geophys. Res*., *103*, 6917–6921, 1998a.

Kamide, Y., et al., Current understanding of magnetic storms: Storm-substorm relationships, *J. Geophys. Res*., *103*, 17,705–17,728, 1998b.

Kappenman, J. G., L. J. Zanetti, and W. A. Radasky, Geomagnetic storm forecasts and the power industry, *Eos Trans. AGU*, *78*, 37–45, 1997.

Kaufmann, R. L., Substorm currents: Growth phase and onset, *J. Geophys. Res*., *92*, 7471–7486, 1987.

Kaye, S. M., R. G. Johnson, R. D. Sharp, and E. G. Shelley, Observations of transient H^+ and O^+ bursts in the equatorial magnetosphere, *J. Geophys. Res*., *86*, 1335–1344, 1981.

Kennel, C. F., and H. E. Petschek, Limit on stably trapped particle fluxes, *J. Geophys. Res*., *71*, 1–28, 1966.

Kintner, P. M., J. Vago, S. Chesney, R. L. Arnoldy, K. A. Lynch, C. J. Pollock, and T. E. Moore, Localized lower hybrid acceleration of ionospheric plasma, *Phys. Rev. Lett*., *68*, 2448–2451, 1992.

Kistler, L. M., F. M. Ipavich, D. C. Hamilton, G. Gloeckler, B. Wilken, G. Kremser, and W. Stüdemann, Energy spectra of the major ion species in the ring current during geomagnetic storms, *J. Geophys. Res*., *94*, 3579–3599, 1989.

Kistler, L. M., E. Möbius, B. Klecker, G. Gloeckler, F. M. Ipavich, and D. C. Hamilton, Spatial variations in the suprathremal ion distribution during substorms in the plasma sheet, *J. Geophys. Res*., *95*, 18,871–18,885, 1990.

Klumpar, D. M., W. K. Peterson, and E. G. Shelley, Direct evidence for a two-stage (bimodal) acceleration of ionospheric ions, *J. Geophys. Res*., *89*, 10,779–10,787, 1984.

Kokubun, S., and R. L. McPherron, Substorm signatures at synchronous altitudes, *J. Geophys. Res*., *86*, 11,265–11,277, 1981.

Konradi, A., C. L. Semar, and T. A. Fritz, Injection boundary dynamics during a geomagnetic storm, *J. Geophys. Res*., *81*, 3851–3865, 1976.

Kozyra, J. U., T. E. Cravens, A. F. Nagy, E. G. Fontheim, and R. S. B. Ong, Effects of energetic heavy ions on electromagnetic ion cyclotron wave generation in the plasmapause region, *J. Geophys. Res*., *89*, 2217–2233, 1984.

Kozyra, J. U., C. E. Rasmussen, R. H. Miller, and L. R. Lyons,

The interaction of ring current and radiation belt protons with ducted plasmaspheric hiss, 1, Diffusion coefficients and timescales, *J. Geophys. Res*., *99*, 4069–4084, 1994.

Kozyra, J. U., C. E. Rasmussen, R. H. Miller, and E. Villalon, Interaction of ring current and radiation belt protons with ducted plasmaspheric hiss, 2, *J. Geophys. Res*., *100*, 21,911–21,919, 1995.

Kozyra, J. U., V. K. Jordanova, R. B. Horne, and R. M. Thorne, Modeling of the contribution of electromagnetic ion cyclotron (EMIC) waves to stormtime ring current erosion, in *Magnetic Storms*, *Geophys. Monogr. Ser*., vol. 98, edited by B. T. Tsurutani et al., pp. 187–202, AGU, Washington, D. C., 1997.

Kremser, G., B. Wilken, G. Gloeckler, D. C. Hamilton, F. M. Ipavich, L. M. Kistler, and P. Tanskanen, Origin, transport, and losses of energetic He^+ and He^{++} ions in the magnetosphere of the Earth: AMPTE/CCE observations, *Ann. Geophys*., *11*, 354–365, 1993.

Krimigis, S. M., G. Haerendel, R. W. McEntire, G. Paschmann, and D. A. Bryant, The Active Magnetospheric Particle Tracer Explorers (AMPTE) program, *Eos Trans. AGU*, *63*, 843–850, 1982.

Krimigis, S. M., G. Gloeckler, R. W. McEntire, T. A. Potemra, F. L. Scarf, and E. G. Shelley, Magnetic storm of September 4, 1984: A synthesis of ring current spectra and energy densities measured with AMPTE/CCE, *Geophys. Res. Lett*., *12*, 329–332, 1985.

Laakso, H., H. Junginger, A. Roux, and R. S. C. DeVilledary, Magnetosonic waves above $f_c(h^+)$ at geostationary orbit: GEOS 2 results, *J. Geophys. Res*., *95*, 10,609–10,621, 1990.

Lanzerotti, L. J., Impacts of solar-terrestrial processes on technological systems, in *Solar-Terrestrial Energy Program*, *COSPAR Colloq. Ser*., vol. 5, edited by D. N. Baker, V. O. Papitashvili, and M. J. Teague, pp. 547–555, Pergamon, Tarrytown, N. Y., 1994.

Lennartsson, W., and E. G. Shelley, Survey of 0.1- to 16-keV/*e* plasma sheet ion composition, *J. Geophys. Res*., *91*, 3061–3076, 1986.

Lewis, Z. V., S. W. H. Cowley, and D. J. Southwood, Impulsive energization of ions in the near-Earth magnetotail during substorms, *Planet. Space Sci*., *38*, 491–505, 1990.

Lindemann, F. A., Note on the theory of magnetic storms, *Philos. Mag*., *38*, 669–1919.

Liu, W. W., and G. Rostoker, Energetic ring current particles generated by recurring substorm cycles, *J. Geophys. Res*., *100*, 21,897–21,910, 1995.

Lockwood, M., Testing substorm theories: The need for multipoint observations, *Adv. Space Res*., *20*(4/5), 883–894, 1997.

Lockwood, M., J. H. Waite Jr., T. E. Moore, J. F. E. Johnson, and C. R. Chappell, A new source of suprathermal O^+ near the dayside polar cap boundary, *J. Geophys. Res*., *90*, 4099–4116, 1985.

Lodge, O., Sunspots, magnetic storms, comet tails, atmospheric electricity and aurorae, *Electrician*, *46*, 249, 1900.

Lu, G., P. H. Reiff, T. E. Moore, and R. A. Heelis, Upflowing ionospheric ions in the auroral region, *J. Geophys. Res*., *97*, 16,855–16,863, 1992.

Ludlow, G. R., Growth of obliquely propagating cyclotron waves in the magnetosphere, *J. Geophys. Res*., *94*, 15,385–15,391, 1989.

Lui, A. T. Y., and D. C. Hamilton, Radial profiles of quiet time magnetospheric parameters, *J. Geophys. Res*., *97*, 19,325–19,332, 1992.

Lui, A. T. Y., R. W. McEntire, and S. M. Krimigis, Evolution of the ring current during two geomagnetic storms, *J. Geophys. Res*., *92*, 7459–7470, 1987.

Lui, A. T. Y., D. J. Williams, E. C. Roelof, R. W. McEntire, and D. G. Mitchell, First composition measurements of energetic neutral atoms, *Geophys. Res. Lett*., *23*, 2641–2644, 1996.

Lui, A. T. Y., R. E. Lopez, B. J. Anderson, K. Takahashi, L. J. Zanetti, R. W. McEntire, T. A. Potemra, D. M. Klumpar, E. M. Greene, and R. Strangeway, Current disruptions in the near-Earth neutral sheet region, *J. Geophys. Res*., *97*, 1461–1480, 1992.

Lundin, R., and L. Eliasson, Auroral energization processes, *Ann. Geophys*., *9*, 202–223, 1991.

Lundin, R., L. R. Lyons, and N. Pissarenko, Observation of the ring current composition at $L < 4$, *Geophys. Res. Lett*., *7*, 425–428, 1980.

Lundin, R., L. Eliasson, and K. Stasiewicz, Plasma energization on auroral field lines as observed by the Viking spacecraft, *Geophys. Res. Lett*., *14*, 443–446, 1987.

Lundin, R., L. Eliasson, G. Haerendel, M. Boehm, and B. Holback, Large-scale auroral plasma density cavities observed by Freja, *Geophys. Res. Lett*., *21*, 1903–1906, 1994.

Lyons, L. R., Pitch angle and energy diffusion coefficients from resonant interactions with ion cyclotron and whistler waves, *J. Plasma Phys*., *12*, 417–432, 1974.

Lyons, L. R., and T. W. Speiser, Evidence for current-sheet acceleration in the geomagnetic tail, *J. Geophys. Res*., *87*, 2276–2286, 1982.

Lyons, L. R., and R. M. Thorne, Parasitic pitch angle diffusion of radiation belt particles by ion cyclotron waves, *J. Geophys. Res*., *77*, 5608–5616, 1972.

Mauk, B. H., Electromagnetic wave energization of heavy ions by the electric "phase branching" process, *Geophys. Res. Lett*., *9*, 1163–1166, 1982.

Mauk, B. H., Quantitative modeling of the convection surge mechanism of ion acceleration, *J. Geophys. Res*., *91*, 13,423–13,431, 1986.

McPherron, R. L., Substorm related changes in the geomagnetic tail: The growth phase, *Planet. Space Sci*., *20*, 1521–1539, 1972.

McPherron, R. L., The role of substorms in the generation of magnetic storms, in *Magnetic Storms*, *Geophys. Monogr. Ser*., vol. 98, edited by B. T. Tsurutani et al., pp. 131–147, AGU, Washington, D. C., 1997.

Meinel, A. B., Doppler shifted auroral hydrogen emission, *Astrophys. J*., *113*, 50–54, 1951.

Milillo, A., S. Orsini, I. A. Daglis, and G. Bellucci, Low-altitude energetic neutral atoms imaging of the inner magnetosphere: A geometrical method to identify the energetic neutral atoms contributions from different magnetospheric regions, *J. Geophys. Res*., *101*, 27,123–27,132, 1996a.

Milillo, A., S. Orsini, I. A. Daglis, and M. Candidi, Ring current ion flows and convection electric field as expected from observations by SAC-B/ISENA, *Geophys. Res. Lett*., *23*, 3285–3288, 1996b.

Milillo, A., S. Orsini, I. A. Daglis, and S. Livi, An empirical model of the energetic ion fluxes in the equatorial inner magnetosphere, *Phys. Chem. Earth*, *24*, 209–214, 1998.

Mizera, P. F., and J. F. Fennell, Signatures of electric fields from high and low altitude particle distributions, *Geophys. Res. Lett*., *4*, 311–314, 1977.

Möbius, E., M. Scholer, B. Klecker, D. Hovestadt, G. Gloeckler, and F. M. Ipavich, Acceleration of ions of ionospheric origin in the plasma sheet during substorm activity, in *Magnetotail Physics*, edited by A. T. Y. Lui, pp. 231–234, Johns Hopkins Univ. Press, Baltimore, Md., 1987.

Moore, T. E., Superthermal ionospheric outflows, *Rev. Geophys*., *22*, 264–274, 1984.

Moore, T. E., and D. C. Delcourt, The geopause, *Rev. Geophys*., *33*, 175–209, 1995.

Moore, T. E., R. L. Arnoldy, J. Feynman, and D. A. Hardy, Propagating substorm injection fronts, *J. Geophys. Res*., *86*, 6713–6726, 1981.

Moritz, J., Energetic protons at low equatorial altitudes: A newly discovered radiation belt phenomenon and its explanation, *J. Geophys*., *38*, 701–717, 1972.

Neugebauer, M., and C. Snyder, The mission of Mariner II: Preliminary observations, *Science*, *138*, 1095–1096, 1962.

Nishida, A., The GEOTAIL mission, *Geophys. Res. Lett*., *21*, 2871–2873, 1994.

Noël, S., A Monte Carlo model of the ring current decay, *Adv. Space Res*., *20*(3), 335–338, 1997a.

Noël, S., Decay of the magnetospheric ring current: A Monte Carlo simulation, *J. Geophys. Res*., *102*, 2301–2308, 1997b.

Orsini, S., I. A. Daglis, M. Candidi, K. C. Hsieh, S. Livi, and B. Wilken, Model calculation of energetic neutral atoms precipitation at low altitudes, *J. Geophys. Res*., *99*, 13,489–13,498, 1994.

Orsini, S., A. Milillo, and M. Candidi, Charge-exchange process in the inner magnetosphere and energetic neutral atoms, in *Fourth International Conference on Substorms* (*ICS-4*), edited by S. Kokobun and Y. Kamide, pp. 791–796, Terra Sci., Tokyo, 1998.

Parker, E. N., Newtonian development of the dynamical properties of the ionised gases at low density, *Phys. Rev*., *107*, 924–933, 1957.

Parker, E. N., Interaction of the solar wind with the geomagnetic field, *Phys. Fluids*, *1*, 171, 1958.

Perreaut, S., Wave-particle interactions in the ULF range: GEOS-1 and -2 results, *Planet. Space Sci*., *30*, 1219–1227, 1982.

Perreaut, S., R. Gendrin, and A. Roux, Amplification of ion cyclotron waves for various typical radial profiles of magnetospheric parameters, *J. Atmos. Terr. Phys*., *38*, 1191–1199, 1976.

Peterson, W. K., E. G. Shelley, S. A. Boardsen, D. A. Gurnett, B. G. Ledley, M. Sugiura, T. E. Moore, and J. H. Waite, Transverse ion energization and low-frequency plasma waves in the mid-altitude auroral zone: A case study, *J. Geophys. Res*., *93*, 11,405–11,428, 1988.

Pfaff, R. F., J. E. Borovsky, and D. T. Young (Eds.), *Measurement Techniques for Space Plasmas: Fields*, *Geophys. Monogr. Ser*., vol. 103, 324 pp., AGU, Washington, D. C., 1998.

Pilipp, W. G., and G. Morfill, The formation of the plasma sheet resulting from plasma mantle dynamics, *J. Geophys. Res*., *83*, 5670–5678, 1978.

Prigancová, A., and Y. I. Feldstein, Magnetospheric storm dynamics in terms of energy output rate, *Planet. Space Sci*., *40*, 581–588, 1992.

Rairden, R. L., L. A. Frank, and J. D. Craven, Geocoronal imaging with Dynamics Explorer, *J. Geophys. Res*., *91*, 13,613–13,630, 1986.

Rauch, J. L., and A. Roux, Ray tracing of ULF waves in a multicomponent magnetospheric plasma: Consequences for the generation mechanism of ion cycltron waves, *J. Geophys. Res*., *87*, 8191–8198, 1982.

Reiff, P. H., H. L. Collin, J. D. Craven, J. L. Burch, J. D. Winningham, E. G. Shelley, L. A. Frank, and M. A. Friedman, Determination of auroral electrostatic potentials using high- and low-altitude particle distributions, *J. Geophys. Res*., *93*, 7441–7465, 1988.

Roederer, J. G., Are magnetic storms hazardous to your health?, *Eos Trans. AGU*, *76*, 441–445, 1995.

Roelof, E. C., Energetic neutral atom image of a storm-time ring current, *Geophys. Res. Lett*., *14*, 652–655, 1987.

Roelof, E. C., Remote sensing of the ring current using energetic neutral atoms, *Adv. Space Res*., *9*(12), 195–203, 1989.

Roelof, E. C., D. G. Mitchell, and D. J. Williams, Energetic neutral atoms ($E \sim 50$ keV) from the ring current: IMP 7/8 and ISEE 1, *J. Geophys. Res*., *90*, 10,991–11,008, 1985.

Roelof, E. C., B. H. Mauk, R. R. Meier, K. R. Moore, and R. A. Wolf, Simulations of EUV and ENA magnetospheric images based on the Rice convection model, in *Instrumentation for Magnetospheric Imagery II*, edited by S. Chakrabarti, *Proc. SPIE Int. Soc. Opt. Eng*., *2008*, 202–213, 1993.

Rostoker, G., E. Friedrich, and M. Dobbs, Physics of magnetis storms, in *Magnetic Storms*, *Geophys. Monogr. Ser*., vol. 98, edited by B. T. Tsurutani et al., pp. 149–160, AGU, Washington, D. C., 1997.

Rothwell, P. L., L. P. Block, M. B. Silevitch, and C.-G. Fälthammar, A new model for substorm onsets: The prebreakup and triggering regimes, *Geophys. Res. Lett*., *15*, 1279–1282, 1988.

Roux, A., S. Perraut, J. L. Rauch, and C. de Villedary, Wave particle interactions near Ω_{He^+} observed on board GEOS 1 and 2, 2, Generation of ion cyclotron waves and heating of He^+ ions, *J. Geophys. Res*., *87*, 8174–8190, 1982.

Russell, C. T., R. E. Holzer, and E. J. Smith, OGO 3 observations of ELF noise in the magnetosphere, 2, The nature of the equatorial noise, *J. Geophys. Res*., *75*, 755–768, 1970.

Schmidt, A., Erdmagnetismus, in *Enzyklopädie der Mathematischen Wissenschaften*, vol. VI, Leipzig, Germany, 1917.

Sckopke, N., A general relation between the energy of trapped particles and the disturbance field over the Earth, *J. Geophys. Res*., *71*, 3125–3130, 1966.

Seki, K., M. Hirahara, T. Terasawa, I. Shinohara, T. Mukai, Y. Saito, S. Machida, T. Yamamoto, and S. Kokubun, Coexistence of Earth-origin O^+ and solar wind-origin H^+/He^{++} in the distant magnetotail, *Geophys. Res. Lett*., *23*, 985–988, 1996.

Shapiro, V. D., G. I. Soloviev, J. Dawson, and R. Bingham, Lower hybrid dissipative cavitons and ion heating in the auroral ionosphere, *Phys. Plasmas*, *2*, 516–526, 1995.

Sheldon, R. B., and D. C. Hamilton, Ion transport and loss in the Earth's quiet ring current, 1, Data and standard model, *J. Geophys. Res*., *98*, 13,491–13,508, 1993.

Shelley, E. G., Magnetospheric energetic ions from the Earth's ionosphere, *Adv. Space Res*., *6*(3), 121–132, 1986.

Shelley, E. G., R. G. Johnson, and R. D. Sharp, Satellite observations of energetic heavy ions during a geomagnetic storm, *J. Geophys. Res*., *77*, 6104–6110, 1972.

Singer, S. F., Trapped orbits in the Earth's dipole field, *Bull. Am. Phys. Soc*., *Ser. II*, *1*, 229, 1956.

Singer, S. F., A new model of magnetic storms and aurorae, *Eos Trans. AGU*, *38*, 175–190, 1957.

Siscoe, G. L., Big storms make little storms, *Nature*, *390*, 448–449, 1997.

Smith, E. J., A. M. A. Frendsen, B. T. Tsurutani, R. M. Thorne, and K. W. Chan, Plasmaspheric hiss intensity variations during magnetic storms, *J. Geophys. Res*., *79*, 2507–2510, 1974.

Smith, P. H., and N. K. Bewtra, Dependence of the charge-exchange lifetimes on mirror altitude, *Geophys. Res. Lett*., *3*, 689–692, 1976.

Smith, P. H., and N. K. Bewtra, Charge exchange lifetimes for ring current ions, *Space Sci. Rev*., *22*, 301–318, 1978.

Smith, P. H., and R. A. Hoffman, Ring current particle distributions during the magnetic storms of December 16–18, 1971, *J. Geophys. Res*., *78*, 4731–4737, 1973.

Smith, P. H., N. K. Bewtra, and R. A. Hoffman, Inference of the ring current ion composition by means of charge exchange decay, *J. Geophys. Res*., *86*, 3470–3480, 1981.

Snyder, C. W., and M. Neugebauer, Interplanetary solar wind measurements by Mariner 2, *Space Res*., *4*, 89, 1964.

Speiser, T. W., Particle trajectories in a model current sheet, based on the open model of the magnetosphere, with applications to auroral particles, *J. Geophys. Res*., *70*, 1717–1728, 1965a.

Speiser, T. W., Particle trajectories in model current sheets, 1,

Analytical solutions, *J. Geophys. Res*., *70*, 4219–4226, 1965b.

Speiser, T. W., and L. R. Lyons, Comparison of an analytical approximation for particle motion in a current sheet with precise numerical calculations, *J. Geophys. Res*., *89*, 147–158, 1984.

Spjeldvik, W. N., and T. Fritz, Theory of charge states of energetic oxygen ions in the Earth's radiation belts, *J. Geophys. Res*., *83*, 1583–1594, 1978.

Størmer, C., *The Polar Aurora*, Oxford Univ. Press, New York, 1955.

Strangeway, R. J., and R. G. Johnson, Mass composition of substorm-related energetic ion dispersion events, *J. Geophys. Res*., *88*, 2057–2064, 1983.

Stuart, G. W., Satellite-measured radiation, *Phys. Rev. Lett*., *2*, 417–418, 1959.

Terasawa, T., et al., Solar wind control of density and temperature in the near-Earth plasma sheet: Wind/Geotail collaboration, *Geophys. Res. Lett*., *24*, 935–938, 1997.

Thelin, B., B. Aparicio, and R. Lundin, Observations of upflowing ionospheric ions in the mid-altitude cusp/cleft region with the Viking satellite, *J. Geophys. Res*., *95*, 5931–5939, 1990.

Thorne, R. M., and R. B. Horne, Cyclotron absorption of ion-cyclotron waves at the bi-ion frequency, *Geophys. Res. Lett*., *20*, 317–320, 1993.

Thorne, R. M., and R. B. Horne, Energy transfer between energetic ring current H^+ and O^+ by electromagnetic ion cyclotron waves, *J. Geophys. Res*., *99*, 17,275–17,282, 1994.

Thorne, R. M., and R. B. Horne, Modulation of electromagnetic ion cyclotron instability due to interaction with ring current O^+ during magnetic storms, *J. Geophys. Res*., *102*, 14,155–14,163, 1997.

Thorne, R. M., E. J. Smith, R. K. Burton, and R. E. Holzer, Plasmaspheric hiss, *J. Geophys. Res*., *78*, 1581–1596, 1973.

Tinsley, B. A., Neutral atom precipitation, *J. Atmos. Terr. Phys*., *43*, 617–632, 1981.

Tinsley, B. A., Solar wind modulation of the global electric circuit and apparent effects on cloud microphysics, latent heat release, and tropospheric dynamics, *J. Geomagn. Geoelectr*., *48*, 165–175, 1996.

Tinsley, B. A., and S.-I. Akasofu, A note on the lifetime of the ring current particles, *Planet. Space Sci*., *30*, 733–740, 1982.

Tsurutani, B. T., W. D. Gonzalez, Y. Kamide, and J. K. Arballo, Preface, in *Magnetic Storms*, *Geophys. Monogr. Ser*., vol. 98, edited by B. T. Tsurutani et al., pp. ix–x, AGU, Washington, D. C., 1997.

Van Allen, J. A., G. H. Ludwig, E. C. Ray, and C. E. McIlwain, Observations of high intensity radiation by satellites 1958 Alpha and Gamma, *Jet Propul*., *28*, 588–592, 1958.

Wahlund, J.-E., and H. J. Opgenoorth, EISCAT observations of strong ion outflows from the *F*-region ionosphere during auroral activity: Preliminary results, *Geophys. Res. Lett*., *16*, 727–730, 1989.

Wahlund, J.-E., H. J. Opgenoorth, I. Häggström, K. J. Winser, and G. O. L. Jones, EISCAT observations of topside ionospheric ion outflows during auroral activity: Revisited, *J. Geophys. Res*., *97*, 3019–3037, 1992.

Wandzura, S., and V. F. Coroniti, Nonconvective ion cyclotron instability, *Planet. Space Sci*., *23*, 123–131, 1975.

Whipple, E. C., (*U*, *B*, *K*) co-ordinates: A natural system for studying magnetospheric convection, *J. Geophys. Res*., *83*, 4318–4326, 1978.

Wilken, B., W. Weiss, D. Hall, M. Grande, F. Søraas, and J. F. Fennell, Magnetospheric Ion Composition Spectrometer onboard the CRRES spacecraft, *J. Spacecr. Rockets*, *29*, 585–591, 1992.

Wilken, B., I. A. Daglis, A. Milillo, S. Orsini, T. Doke, S. Livi, and S. Ullaland, Energetic neutral atoms in the outer magnetosphere: An upper flux limit obtained with the HEP-LD spectrometer on board GEOTAIL, *Geophys. Res. Lett*., *24*, 111–114, 1997.

Williams, D. J., Ring current composition and sources, in *Dynamics of the Magnetosphere*, edited by S.-I. Akasofu, pp. 407–424, D. Reidel, Norwell, Mass., 1980.

Williams, D. J., Ring current composition and sources: An update, *Planet. Space Sci*., *29*, 1195–1203, 1981.

Williams, D. J., The Earth's ring current: Causes, generation, and decay, *Space Sci. Rev*., *34*, 223–234, 1983.

Williams, D. J., Ring current and radiation belts, *U.S. Natl. Rep. Int. Union Geod. Geophys. 1983–1986*, *Rev. Geophys*., *25*, 570–578, 1987.

Williams, D. J., Why we need global observations, in *Magnetospheric Physics*, edited by B. Hultqvist and C. G. Fälthammar, pp. 83–101, Plenum, New York, 1990.

Williams, D. J., E. C. Roelof, and D. G. Mitchell, Global magnetospheric imaging, *Rev. Geophys*., *30*, 183–208, 1992.

Wodnicka, E. B., and M. Banaszkiewicz, The features of the auroral topside ionosphere-magnetosphere coupling induced by the time-dependent magnetic field, *Adv. Space Res*., *18*(9), 87–90, 1996.

Wodnicka, E. B., and M. Banaszkiewicz, Outflowing ionospheric oxygen-ion motion in a reconfigurating magnetosphere, *Ann. Geophys*., *15*, 5–16, 1997.

Wolf, R. A., J. W. Freeman Jr., B. A. Hausmann, R. W. Spiro, R. V. Hilmer, and R. L. Lambour, Modeling convection effects in magnetic storms, in *Magnetic Storms*, *Geophys. Monogr. Ser*., vol. 98, edited by B. T. Tsurutani et al., pp. 161–172, AGU, Washington, D. C., 1997.

Yau, A. W., B. A. Whalen, W. K. Peterson, and E. G. Shelley, Distribution of upflowing ionospheric ions in the high-altitude polar cap and auroral ionosphere, *J. Geophys. Res*., *89*, 5507–5522, 1984.

Yau, A. W., E. G. Shelley, W. K. Peterson, and L. Lenchyshyn, Energetic auroral and polar ion outflow at DE-1 altitudes: Magnitude, composition, magnetic activity dependence, and long-term variations, *J. Geophys. Res*., *90*, 8417–8432, 1985.

Yau, A. W., E. G. Shelley, and W. K. Peterson, Accelerated auroral and polar-cap ions: Outflow at DE-1 altitudes, in *Ion Acceleration in the Magnetosphere and Ionosphere*, *Geophys. Monogr. Ser*., vol. 38, edited by T. Chang, pp. 72–76, AGU, Washington, D. C., 1986.

Yeh, H.-C., and J. C. Foster, Storm time ion outflow at mid-latitude, *J. Geophys. Res*., *95*, 7881–7891, 1990.

W. Baumjohann, Max-Planck-Institut für Extraterrestrische Physik, P.O. Box 1603, 85740 Garching, Germany.

I. A. Daglis, Institute of Ionospheric and Space Research, National Observatory of Athens, Metaxa and Vas. Pavlou Streets, 15236 Penteli, Greece (daglis@creator.space.noa.gr)

S. Orsini, Istituto de Fisica dello Spazio Interplanetario, Consiglio Nazionale delle Ricerche, Via del Fosso del Cavaliere, 00133 Roma, Italy.

R. M. Thorne, Department of Atmospheric Sciences, University of California, Los Angeles, CA 90024.